

See discussions, stats, and author profiles for this publication at: <https://www.researchgate.net/publication/391927964>

# A photonic toroidal vortex model of the hydrogen atom fine structure

Article in *Quantum Studies Mathematics and Foundations* · May 2025

DOI: 10.1007/s40509-025-00364-9

---

CITATIONS

0

READS

25

1 author:



**Barry R Clarke**

Brunel University London

28 PUBLICATIONS 20 CITATIONS

SEE PROFILE

# A PHOTONIC TOROIDAL VORTEX MODEL OF THE HYDROGEN ATOM FINE STRUCTURE

BARRY R. CLARKE

*Independent researcher*

*aleteller@barryispuzzled.com*

The calculation of the fine structure hydrogen energy levels for both the classical Sommerfeld and the quantum mechanical Dirac models relies on the specification of an external potential. However, recent experimental evidence has shown that electrons can adopt quantized orbital states even when there is no external potential. So a revised approach is required and suggested. Using the latest research on optical spin angular momentum (SAM) and optical orbital angular momentum (OAM), a novel reworking of the classical Sommerfeld model is carried out in terms of a photonic toroidal vortex (PTV). A construction for both an electron and proton mass is presented based on OAM, the difference being only one of scale. When the OAM is curved into a PTV, an internal potential can be defined for the orbiting electron based on the toroidal rotation energy. Using an electron and a proton both in the form of a PTV, a bound state model of the hydrogen atom can be formed. An opportunity presents itself to define concepts such as mass, magnetic momentum, and electric momentum in terms of the poloidal and toroidal rotations of a PTV. A derivation of Coulomb's law is given using vector line integrals. Fine structure energy states with reduced mass are given for the first six states of each of the following  $nS_{1/2}$ ,  $nP_{1/2}$ ,  $nP_{3/2}$ ,  $nD_{3/2}$ , and  $nD_{5/2}$ , to an accuracy of less than 2 parts in  $10^{10}$  for all levels compared with the Sommerfeld–Dirac energies.

*Keywords: photonics; optical spin angular momentum, optical orbital angular momentum; photonic toroidal vortex; hydrogen atom; fine structure*

## CONTENTS

1. Introduction	2	2.7.2. Momentum fields	12
1.1 Structure of a photon	2	2.7.3. Self-potential	13
1.2 The proposed PTV model	3	2.7.4. Field structure	13
2. The ‘unloaded’ PTV model	4	3. The ‘loaded’ PTV model	15
2.1. Sp-1 rotation (optical SAM)	4	3.1. The notional tube	15
2.2. Sp-2 rotation (optical OAM)	5	3.2. Fine-structure formula	15
2.2.1. Definition of rest mass	5	3.2.1. The mass formula	15
2.2.2. Linear momentum	6	3.2.2. Sp-2 and Sp-3 speed	16
2.3. Attraction energy	6	3.2.3. Sp-2 and Sp-3 momentum	17
2.3.1. Total Sp-2 energy	6	3.2.4. Energy of Sp-3 motion	17
2.3.2. Distance transformation	6	3.2.5. Sommerfeld–Dirac energy levels	17
2.3.3. Total single-HS action	7	3.2.6. Sp-3 radial and intensity functions	19
2.3.4. Radius transformation	7	3.2.7. Sp-2 action	21
2.3.5. Time period	7	4. The Hydrogen atom	22
2.3.6. Passive acceleration	7	4.1. Coulomb's law for bound states	22
2.4. Repulsion energy	8	4.2. State boundaries	25
2.4.1. Total Sp-2 energy	8	4.3. Reduced mass	26
2.4.2. Momentum	8	5. Conclusions	27
2.4.3. Time-period transformation	8	Appendix	29
2.4.4. Radius transformation	8	References	29
2.4.5. Total single-HS action	9		
2.4.6. Active acceleration	9		
2.5. The spiral magnetic-momentum field	10		
2.6. Response to fields	11		
2.7. Sp-3 rotation (toroidal)	11		
2.7.1. PTV construction	11		

# 1. INTRODUCTION

## 1.1. Structure of a photon

Bohr's model of the hydrogen atom combined the particle theory of Newton with the quantization rules of the old quantum theory to account for its stable discrete energy levels [1]. The generalization to elliptic orbits by Sommerfeld subsequently predicted a fine structure with  $(2n + 1)$  energy levels for each Bohr state [2]. However, it was Dirac's relativistic quantum mechanics of the electron [3] that allowed Darwin to derive a modification to Sommerfeld's fine-structure formula [4]. Here, the concept of doublets described by a half-number  $j$  was introduced,<sup>1</sup> in which energy values for the same  $j$  but different  $l$  are degenerate. However, when the  $n = 2$  Dirac fine-structure states were examined with microwave radiation the  $2S_{1/2}$  energy was found to differ from the  $2P_{1/2}$  by approximately 1000 MHz [5]. Bethe *et al.* [6] subsequently calculated the Lamb shift to be 1051.41 MHz against the best modern experimental value of 1057.845 MHz [7].

Both the Sommerfeld and Dirac theories of fine structure employ the methods of Lagrange and Hamilton in which the specification of an *external* potential obtains a reasonable agreement of the energy levels with observation. However, experiments on electron vortices in transmission electron microscopes have shown that electrons can be prepared in quantized orbital states with large OAM, in free space devoid of any central potential, electromagnetic field, or medium that confines the orbits [8–10]. In fact, values of OAM in electron vortex beams have been generated up to  $|l| = 100$  *without* an external potential [10]. A vortex beam adopts a screw-type structure possessing a wavefront with a quantized topological form and a singularity in phase of the form  $e^{il\phi}$ , where  $\phi$  is the angle about the beam axis and  $l$  is an integer quantum number. Since the Sommerfeld–Dirac approaches to the production of electron energy levels relies on an *external* potential, the model presented here will consist of a modification of the classical Sommerfeld approach to fine structure, with the introduction of an *internal* potential, presented in the context of a curved OAM trajectory in the form of a photonic toroidal vortex (PTV) model. For a comprehensive quantum mechanical review of the theory and applications of free-electron vortex states with OAM, see Lloyd *et al.* [11] and Bliokh *et al.* [12].

Some interesting investigations have been carried out into the structure of a single photon. Not only can it possess spin angular momentum (SAM) [13–17], but optical elements such as spiral wave-plates [18], holograms [19–21], and cylindrical lenses [22–25] have been used to divert the linear geometrical-optics rays of the SAM into a helical phase structure as optical OAM, see Fig. 1. When the wave equation is solved in cylindrical coordinates  $(r, \phi, z)$  in field-free space, for a propagation along the  $z$  axis we have  $\psi(\mathbf{r}) \propto f(\mathbf{r})\exp(ik_z z + il\phi)$ , where  $k_z$  is the longitudinal wave number,  $l \in \mathbb{Z}$  is the azimuthal quantum number, and  $f(\mathbf{r})$  is a slowly-changing radial distribution. Vortex beams arise from  $l \neq 0$  with an OAM per photon of  $l\hbar$  [12]. The literature on optical OAM is extensive [26–43].

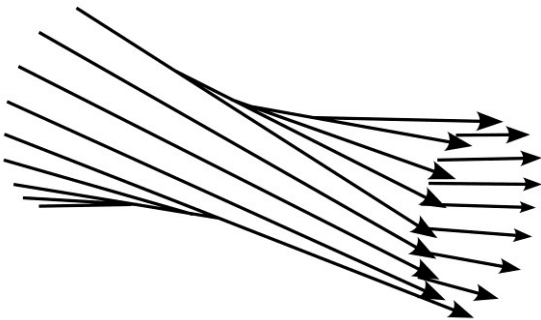


FIG. 1. Optical OAM constructed from diverting linear geometrical-optics rays of SAM with phase dependent on azimuthal angle.

Coincidence-counting in SPDC-generated photon experiments have seemingly brought out both the particle and wave aspects of a photon [44–50]. From the calculated value of the second-order correlation function,

<sup>1</sup>  $j = (l - 1) + 1/2$  and  $j = l + 1/2$ , for  $l = 0, 1, \dots, (n - 1)$ , the orbital quantum number.

arguments are usually made that a single photon can be detected once only.<sup>2</sup> However, simultaneous detector registrations actually occur, and a reinterpretation of the results has been advanced in which there is a propagating single-photon front that takes the form of a transversely-iterated non-rotating array of phase-matched helical strings (HS) [51]. This transverse structure can be used to construct a single-photon OAM. Each HS in the front is capable of registration at a detector but the suggestion has been made that two separate detectors can be triggered by different HS in the same single-photon front with a probability that can be as low as  $7.5 \times 10^{-4} - 5.3 \times 10^{-2}$  for the experiments examined.<sup>3</sup> So, a multiple triggering of detectors from a single-photon front *can* exhibit itself but it does so infrequently. In the present model, we take an electron and proton to consist of a HS diverted into OAM but with one significant difference. Here, our SAM axis will be curvilinear rather than a diversion of the linear trajectories across the transverse front, see Fig. 1. A PTV is then to consist of the curved trajectory of the OAM axis and this will also be the form that an orbiting electron and proton take on in a hydrogen bound state.

Optical OAM has recently been transformed into a photonic toroidal vortex (PTV) [52]. A fibre laser acts as the source of longitudinally iterated photons that separate into a reference pulse and a signal pulse, see Fig. 2. The former is dechirped<sup>4</sup> to a transform-limited pulse<sup>5</sup> through a grating pair, while the latter passes through a 2-D pulse shaper.<sup>6</sup> Moving a reflective mirror allows the path length difference between the reference and signal to be varied. After undergoing a spatio-temporal Fourier transform, the signal pulse is converted to a wave packet carrying a spatio-temporal vortex (STOV). It is then stretched along the vortex line using an afocal cylindrical beam expander before passing through spatial light modulators (SLM) to form an afocal mapping system. These SLM are programmed with phase profiles, and the stretched spatio-temporal vortex transforms into a toroidal vortex through the conformal mapping system. Its recombination with the reference pulse in a CCD camera brings out an interference pattern.

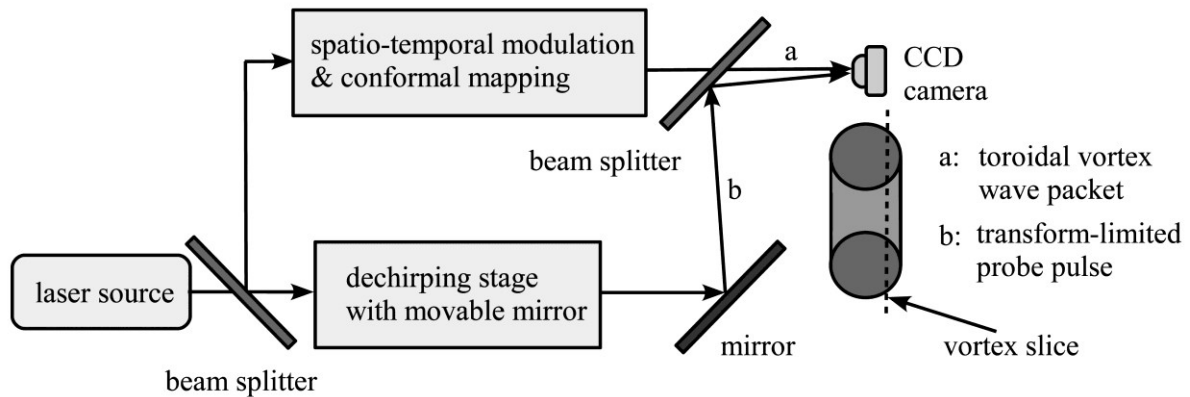


FIG. 2. Schematic diagram showing the creation of a toroidal vortex [52]. The signal pulse takes the upper path and the reference pulse takes the lower path.

## 1.2. The proposed PTV model

The present work recasts the classical Sommerfeld theory into a PTV model. It examines how optical OAM might provide the basis for definitions of mass and magnetic momentum, while its trajectory around a PTV might allow an insight into the concepts of charge, electric momentum, and consequently electric field potential. There will be no difference in the structure of an electron and proton, the former being a scaled-up version of the latter. A single-photon front (array of HS) — see Figs 3 and 4 — is to rotate on the surface of a PTV at the

<sup>2</sup> It remains a fact that a small second-order correlation function result  $0 < \alpha \ll 1$  does *not* demonstrate an absence of coincidences. The value of  $\alpha$  is not zero.

<sup>3</sup> A single HS induces circular polarization — optical SAM — in a stationary plane set perpendicular to the optic axis.

<sup>4</sup> In an up-chirped pulse, the frequency increases with time over the pulse duration. For a down-chirped pulse, the frequency decreases with time. The effect can be reduced by propagating it through optical components with suitable chromatic dispersion (external modulator).

<sup>5</sup> A transform-limited pulse has a minimum possible duration for a given spectral bandwidth, with a constant phase across all frequencies constituting the pulse which is generated by mode-locked lasers. The dispersion of the medium must be zero to keep the pulse together otherwise there are spectral phase changes.

<sup>6</sup> A grating, cylindrical lens, and reflective programmable spatial light modulator induces a spiral phase in the signal pulse.

speed of light. In contrast to traditional electrodynamics [53], the HS is not constructed from vibrating electric and magnetic fields. Instead, the linear momentum of the HS is the resultant of two rotating components: optical OAM or magnetic momentum (poloidal rotation in a PTV); and electric momentum (toroidal rotation in a PTV). We suggest that each rotation generates a spiral momentum field, the former being magnetic and the latter electric. As experiment requires [8–10], such PTVs possess the property that they can take on quantized energy levels in a field-free space. This is not a feature of the Sommerfeld–Dirac schemes.

In Section 2.7.3, a self-potential or internal potential is introduced in the form of toroidal rotation. This allows us to set up an ‘unloaded’ PTV, that is, one that has absorbed no radiation. After discussing the spiral fields, in Section 3 a ‘loaded’ PTV is constructed, that is, one that has absorbed radiation. The hydrogen bound state is to consist of a proton and electron PTV coaxially aligned in close proximity, see Section 4. The proton’s electric-momentum field inhabiting the electron PTV displaces part of the latter’s toroidal energy into energy of motion towards the proton. It is this energy of motion that is radiated away at a state boundary, bringing the electron to rest with respect to the proton, and creating a stationary bound state. The agreement with the Sommerfeld–Dirac fine structure formula is better than 2 parts in  $10^{10}$  for all states, before an adjustment for reduced mass is derived from the theoretical assumptions in Section 4.2. Appendix A contains all the data used in the calculations.

## 2. THE ‘UNLOADED’ PTV MODEL

### 2.1. Sp–1 rotation (optical SAM)

Before the fine structure series can be derived, a PTV is to be constructed that has been formed without radiation absorption. This might occur when an electron or proton — which is to be defined using optical OAM in Section 2.2.1 — meets a repulsive field and its trajectory is provided with curvature. Based on coincidence registrations recorded in spontaneous parametric down-conversion (SPDC) photon-counting experiments, the following model of a *single* photon has been suggested [51]. A HS of wavelength  $\lambda_1$  consists of a string of length  $\sqrt{2}\lambda_1$  with rake  $\pi/4$ , see Fig. 3. This string is wound round a notional tube that is non-rotating and travelling linearly at speed  $v_1 = c$  along its propagation axis. The azimuthal momentum or optical spin angular momentum (SAM) that the HS induces in a stationary plane set perpendicular to the propagation axis is to be denoted as Sp-1.<sup>7</sup> This is also known as right- or left-circular polarization for a left- or right-wound string, respectively. At a rake of  $\pi/4$  the wavelength is  $\lambda_1 = 2\pi r_1$ , where  $r_1$  is the tube radius, while both the linear and azimuthal momentum at a rake of  $\pi/4$  are  $p_1 = h/\lambda_1$ . This is consistent with Poynting’s model in which he gives the relationship of the wavelength  $\lambda$  to the circular polarization radius  $a$  as  $\tan \epsilon = 2\pi a/\lambda$ , where  $\epsilon$  is the angle between the tangent to the helix and its axis [54].<sup>8</sup>

It has been suggested that a *single* photon is to consist of an array of HS with parallel axes, transversely iterated threads possessing substance and an identical phase across the propagation front, see Fig. 4 [51]. In this way, an array of circular paths is traced out in the plane by an array of points as the single photon passes through. Although multiple triggering of detectors is possible from a single photon array, whether or not coincident registrations occur must depend on the absorption characteristics of the target surface. The probability of a double registration in the experiments performed appears to be as low as  $7.5 \times 10^{-4} - 5.3 \times 10^{-2}$  [51]. Linear polarization arises from the superposition of coaxial and oppositely wound strings with the same wavelength, which nullifies the SAM and allows only linear momentum to be conveyed perpendicular to the plane. A string that is longitudinally iterated with length  $n\lambda_1$  and phase-matched ends consists of  $n$  photons with total linear momentum  $np_1$ .

<sup>7</sup> This is not to be confused with quantum mechanical spin. Also, the helical string does not possess Sp-1, but generates the rotation in a material it passes through.

<sup>8</sup> An alternative model of a HS seems feasible in which a string of length  $\sqrt{2}\lambda_1$  travels along a helical trajectory at speed  $\sqrt{2}c$  with rake  $\pi/4$  so that both the linear and azimuthal components have speed  $c$ . In this case, the string would actually possess Sp-1.

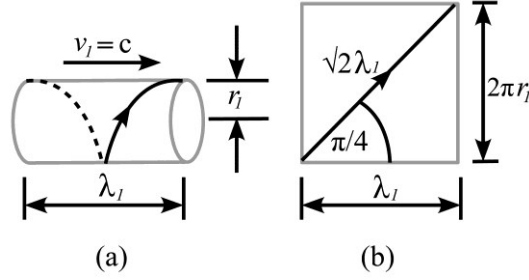


FIG. 3. A single Sp-1 notional tube. (a) Left-wound single-wavelength HS running around a notional tube with radius  $r_1$  and advancing at speed  $v_1 = c$ . (b) Net of the unwound string and tube with rake  $\pi/4$  showing that  $\lambda_1 = 2\pi r_1$ .

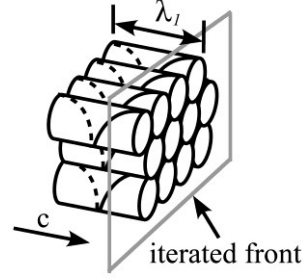


FIG. 4. Transversely iterated array of left-wound HS on the surface of notional guide tubes with wavelength  $\lambda_1$  moving at speed  $c$ . The helices shown have equal phase on the front and produce right-circular polarization in the plane [51].

## 2.2. Sp-2 rotation (optical OAM)

### 2.2.1. Definition of rest mass

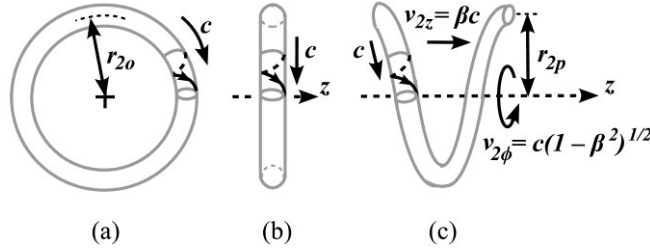


FIG. 5. Construction of a Sp-2 helix (optical OAM) from a HS. (a) The HS in Fig. 3 is diverted into a closed circle of Sp-2 radius  $r_{2o}$ , see Eq. (8) and Section 2.3.6. (b) Right-end elevation of Fig. 5(a). (c) The Sp-2 ring in Fig. 5(b) is sliced through its cross-section and uncoiled so that a helical trajectory is adopted without the addition of energy. The string follows the Sp-2 guide tube at speed  $c$  and moves at speed  $v_{2z}$  along its optic axis  $z$ , where  $\beta = v_{2z}/c$ . Its passive acceleration radius is  $r_{2p}$ .

Let the HS now adopt a circular trajectory with radius  $r_{2o}$ , such that the axis is along the  $z$  axis. This has no linear momentum, only azimuthal momentum  $p_{2\phi o} = \hbar/r_{2o}$  and speed  $c$ , see Figs 5(a) and 5(b). This rotation around the  $z$  axis shall be denoted Sp-2.<sup>9</sup> While optical OAM has been produced in the laboratory by diverting linear rays with optical elements (see Fig. 1), we suggest that our OAM curvature is likely created at the nuclear level by magnetic fields, see Fig. 5.

Slater's attempt at defining 'mass' gives the structure of an electron as "[...] an energyless field from a point charge and [magnetic] doublet, with the energy and angular momentum located in the quantum [attached to it] travelling with the speed of light in a circle [to which Poynting's vector is tangential] of radius  $r_o$  [...] satisfying the condition that the electric field at this distance,  $e/r_o^2$ , should equal in magnitude the magnetic field,

<sup>9</sup> Unlike Sp-1 as defined in Section 2.1, the HS actually *possesses* Sp-2 rotation.

$eh/4\pi mcr_o^3$ , which gives [for the electron]  $r_o = h/4\pi mc = 1.93 \times 10^{-11}$  cm” [55]. Our definition of rest mass  $m_o$  is also to depend on a radius  $r_{2o}$ , or more specifically string length  $l_{2o}$ , thus

$$m_o = \frac{h}{2\pi r_{2o} c} = \frac{h}{l_{2o} c} \quad (1)$$

A trapped single HS confined to a circular trajectory with Sp-2 radius  $r_{2o} = 3.861\,592\,68 \times 10^{-13}$  m — twice Slater’s value — gives the value of the electron rest mass. Similarly, a proton with rest mass  $m'_o$  occurs at Sp-2 radius  $r'_{2o} = 2.103\,089\,104 \times 10^{-16}$  m. OAM beam waists created in the laboratory from optical elements are typically much larger than this. For example, Friese *et al.* [56] report using  $r = 2 \times 10^{-6}$  m while Leach *et al.* [41] have produced  $r = 10^{-3}$  m. In what follows, we shall consistently adopt unprimed variables for the electron, and primed variables for the proton.

### 2.2.2 Linear momentum

Without adding energy, let us now impart linear momentum to the HS by slicing through its cross-section and uncoiling it along the  $z$  axis. It now takes on a helical trajectory, see Fig. 5(c).<sup>10</sup> The velocity vector is

$$\vec{v}_2 = \begin{pmatrix} v_{2\phi} \\ v_{2z} \end{pmatrix} = c \begin{pmatrix} (1 - \beta^2)^{1/2} \\ \beta \end{pmatrix} \quad (2)$$

where  $\beta = v_{2z}/c$ .<sup>11</sup> Since no energy is absorbed, the string length  $l_{2o}$  and mass  $m_o$  remain unchanged. So, for an electron, the Sp-2 momentum vector is

$$\vec{p}_2 = m_o \begin{pmatrix} v_{2\phi} \\ v_{2z} \end{pmatrix} = m_o c \begin{pmatrix} (1 - \beta^2)^{1/2} \\ \beta \end{pmatrix} \quad (3)$$

where  $m_o$  is defined in Eq. (1) in terms of string length. Here, the Sp-2 velocity vector  $\vec{c}$  for the rest mass has been redirected to provide motion along the  $z$  axis.

## 2.3. Attraction energy

### 2.3.1. Total Sp-2 energy

The term ‘attraction energy’ is used to signify that no energy is absorbed by the PTV. It is merely redistributed. The invariant electron energy  $\mathcal{E}$  results from the scalar product of Eqs. (2) and (3) as an action per unit time thus

$$\mathcal{E} = \vec{p}_2 \cdot \vec{v}_2 = m_o c \begin{pmatrix} (1 - \beta^2)^{1/2} \\ \beta \end{pmatrix} \cdot \begin{pmatrix} (1 - \beta^2)^{1/2} \\ \beta \end{pmatrix} c = m_o c^2 \quad (4)$$

Again, since the length is kept constant when uncoiling the string then the mass remains constant.

### 2.3.2 Distance transformation

Since  $T_o = 2\pi r_{2o}/c$ , where  $T_o$  is the time period of the circular trajectory, then since the distance travelled by the HS along the string and the time period remain unchanged by the uncoiling, the distance travelled azimuthally  $d_\phi$  and linearly  $d_z$  must be proportional to the speed in those directions, see Eq. (2). So

<sup>10</sup> Researchers still employ the language of electric- and magnetic-field vectors when discussing a photon by referring to the trajectory of the Poynting vector [42].

<sup>11</sup> Slater also thought that the Poynting vector direction had to allow the electron to “transform as a velocity under the Lorentz transformation” [55].

$$\begin{pmatrix} d_\phi \\ d_z \end{pmatrix} = c \begin{pmatrix} (1 - \beta^2)^{1/2} \\ \beta \end{pmatrix} T_o = \begin{pmatrix} (1 - \beta^2)^{1/2} \\ \beta \end{pmatrix} 2\pi r_{2o} \quad (5)$$

### 2.3.3. Total single-HS action

With no absorption of action, the total action is invariant, so that the azimuthal action around the Sp-2 axis is reduced from  $h$  and the loss is redistributed into linear action as follows:

$$h = m_o \begin{pmatrix} v_{z\phi} \\ v_{zz} \end{pmatrix} \cdot \begin{pmatrix} d_\phi \\ d_z \end{pmatrix} = m_o c \begin{pmatrix} (1 - \beta^2)^{1/2} \\ \beta \end{pmatrix} \cdot \begin{pmatrix} (1 - \beta^2)^{1/2} \\ \beta \end{pmatrix} 2\pi r_{2o} \quad (6)$$

which recovers Eq. (1). In Section 4.1.1, we derive Coulomb's law and assume that this redistribution occurs when an external attractive field, with a field momentum that has opposite rotation to the resident toroidal rotation (Sp-3), displaces toroidal energy into linear energy of motion without any change in the total energy.

### 2.3.4. Radius transformation

From Eq. (5), setting the azimuthal distance  $d_\phi = 2\pi r_{2p}$ , the Sp-2 radius transforms as follows:

$$r_{2p} = (1 - \beta^2)^{1/2} r_{2o} \quad (7)$$

where  $r_{2p}$  is the Sp-2 passive acceleration radius, see Sec. 2.3.6.

### 2.3.5. Time-period

The time period of one complete cycle is obtained from Eq. (1) with  $T_{2o} = 2\pi r_{2o}/c$  so that

$$T_{2o} = \frac{h}{m_o c^2} \quad (8)$$

### 2.3.6. Passive acceleration

Traditionally, when a body is accelerated, the cause is an absorption of energy. However, it is possible to observe a body accelerate that is not absorbing energy. This observation would be taken from the standpoint of an accelerating body that itself has received energy. In this respect, when discussing acceleration, there needs to be a distinction between a body that receives energy and one that does not. Consider two electron Sp-2 loops as reference frames  $S$  and  $S'$  which are at rest with respect to each other, see Fig. 6(a). A circularly polarized photon strikes the electron in  $S'$  and it accelerates along the positive  $z$  axis. We ask how the trajectory of  $S$ , which absorbs no energy, will appear when viewed from  $S'$ , see Fig. 6(b). Having absorbed no energy, the velocity and momentum vectors are given by Eqs. (2) and (3), and the total invariant energy by Eq. (4). This type of acceleration will be denoted as *passive*, in that its acquisition of acceleration is not accompanied by the absorption of energy.

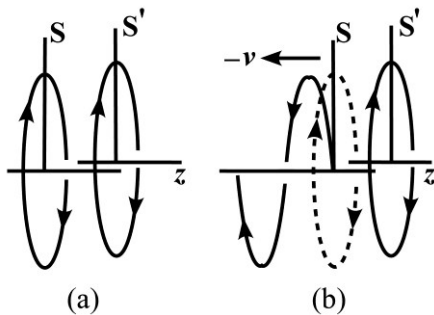


FIG. 6 (a) Two electrons (Sp-2 or optical OAM) in frames of reference  $S$  and  $S'$  at rest with respect to each other. (b) The electron in frame  $S'$  absorbs energy to ‘actively’ accelerate to speed  $v$  along the positive  $z$  axis and views the electron in  $S$  that has absorbed no energy ‘passively’ accelerating to speed  $(-v)$  without absorbing energy. Frame  $S'$  *must* regard the total energy of the electron  $S$  as given by Eq. (4).

## 2.4. Repulsion energy

### 2.4.1 Total Sp-2 energy

Let us suppose there is an addition of energy, not from radiation but from a repulsion field, to produce the trajectory in Fig. 5(c) — albeit with a different radius. This addition, which here arises from a same sense field rotation that overloads the azimuthal action, becomes redistributed into linear energy of motion. First, we partition the square of the light speed as follows:

$$c^2 = c^2(1 - \beta^2) + \beta^2 c^2 \quad (9)$$

Multiplying by  $m_o^2$  and dividing by  $(1 - \beta^2)$  to increase the mass gives

$$m_2^2 c^2 = m_o^2 c^2 + m_2^2 \beta^2 c^2, \quad m_2 = \frac{m_o}{(1 - \beta^2)^{1/2}}, \quad |\vec{p}| = m_2 \beta c \quad (10)$$

After rearrangement we obtain the energy–momentum equation

$$\frac{\mathcal{E}^2}{c^2} - \vec{p} \cdot \vec{p} = m_o^2 c^2, \quad \mathcal{E} = m_2 c^2 \quad (11)$$

For ways in which we propose that energy can interact with an Sp-2 circuit, see Section 4.1.1.

### 2.4.2 Momentum

While the velocity vector follows Eq. (2), the Sp-2 or magnetic momentum vector is similar to Eq. (3) as follows:

$$\vec{p}_2 = m_2 \begin{pmatrix} v_{2\phi} \\ v_{2z} \end{pmatrix} = m_2 c \begin{pmatrix} (1 - \beta^2)^{1/2} \\ \beta \end{pmatrix} \quad (12)$$

Here, we obtain the mass  $m_2$  from Eq. (10), and from Eq. (2) the speed in the azimuthal direction is  $c(1 - \beta^2)^{1/2}$ .

### 2.4.3 Time-period transformation

The suggestion made here is that a repulsion field overloads the Sp-2 action and redistributes the excess into linear action along the  $z$  axis, returning the azimuthal action to  $h$ . Since the azimuthal action is to be an invariant, we can find the time period  $T$  for the added-energy case by dividing the action by the azimuthal energy thus

$$T_2 = \frac{h}{m_2 c^2 (1 - \beta^2)} \quad (13)$$

Combining Eq. (8) with the mass from Eq. (10), we have

$$T_2 = \frac{T_{2o}}{(1 - \beta^2)^{1/2}} \quad (14)$$

This means that considered from a non-rotating frame, for the active acceleration (energy absorbed) case, the Sp-2 ring (which is the form of an electron or proton) *absolutely* takes longer to complete one revolution than the passive (non-absorption) case.

#### 2.4.4 Radius transformation

We only need to take the velocity vector from Eq. (2) and the energy-absorbed time period from Eq. (14) to find the distance travelled in the azimuthal and  $z$  directions, thus

$$\begin{pmatrix} d_\phi \\ d_z \end{pmatrix} = \begin{pmatrix} v_{2\phi} \\ v_{2z} \end{pmatrix} T_2 = c \begin{pmatrix} (1 - \beta^2)^{1/2} \\ \beta \end{pmatrix} \frac{T_{2o}}{(1 - \beta^2)^{1/2}} \quad (15)$$

so that  $d_\phi = cT_{2o} = 2\pi r_{2o} = 2\pi r_{2a}$ , where  $r_{2a}$  is the active acceleration tube radius. From Eq. (5) in the passive case,  $d_\phi = (1 - \beta^2)^{1/2} 2\pi r_{2o} = 2\pi r_{2p}$ . So

$$r_{2a} = \frac{r_{2p}}{(1 - \beta^2)^{1/2}} = r_{2o} \quad (16)$$

Comparison with Eq. (7) shows that the active acceleration tube radius  $r_{2a}$  is the same as for the stationary Sp-2 ring  $r_{2o}$ .

#### 2.4.5 Total single-HS action

Let us take the scalar product of momentum from Eq. (12) with velocity from Eq. (2) and multiply by the time from Eq. (14) to find the action

$$J = m_2 c \begin{pmatrix} (1 - \beta^2)^{1/2} \\ \beta \end{pmatrix} \cdot \begin{pmatrix} (1 - \beta^2)^{1/2} \\ \beta \end{pmatrix} c T_2 = \frac{m_o c^2 T_{2o}}{(1 - \beta^2)} \begin{pmatrix} (1 - \beta^2)^{1/2} \\ \beta \end{pmatrix} \cdot \begin{pmatrix} (1 - \beta^2)^{1/2} \\ \beta \end{pmatrix} \quad (17)$$

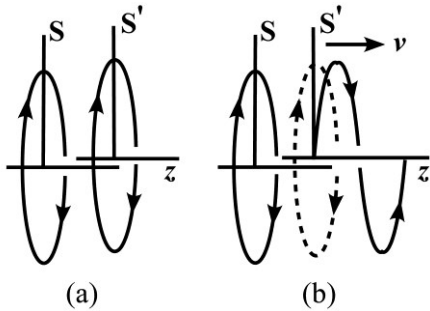
having used Eq. (10) for  $m_2$ . Using Eq. (8), the azimuthal action is

$$J_\phi = m_o c^2 T_{2o} = h \quad (18)$$

So when energy is absorbed by an electron or proton, either by a same sense rotating momentum field or a same sense circularly polarized photon, the azimuthal action is invariant, the Sp-2 radius remains unchanged, and the overloading action is redistributed into linear action as motion.<sup>12</sup>

#### 2.4.6 Active acceleration

We now ask how the HS trajectory of  $S'$  appears in the frame of  $S$ . Electron  $S'$  has *absolutely* gained energy — that is, all non-rotating frames of reference can agree that an absorption event has occurred. However, it has been redirected out of the ring plane into linear motion, see Fig. 7(b). The total energy is given by Eq. (11).



<sup>12</sup> In a paper in progress dealing with the hyperfine level separation, it will be argued that moving magnetic momentum field lines cutting an Sp-2 circuit can also change its energy.

FIG. 7. (a) Two electrons in frames of reference  $S$  and  $S'$  at rest with respect to each other. (b) The electron in frame  $S'$  absorbs energy to actively accelerate to speed  $v$  along the positive  $z$  axis and frame  $S$  views the transaction of this energy.

This type of acceleration, the only one considered in physics at present, will be denoted as *active*. It should be clear from the comparison of time periods in Eq. (14) that the actively accelerated ring will complete its azimuthal rotation through  $2\pi$  radians *after* the passively accelerated one, in *any* non-rotating observation frame. This surely has consequences for the relativistic twin paradox which we shall explore no further here.

## 2.5. The spiral magnetic-momentum field

Leach *et al.* [41] have succeeded in measuring the skew angle of the Poynting vector for optical OAM, denoted here as Sp-2. For this, they used a multi-photon laser-generated helically phased beam with a Shack-Hartmann wave-front sensor. They report that the following radial, azimuthal, and linear momentum densities apply

$$\begin{aligned} p_r &= \varepsilon_o \frac{\omega k r z}{(z^2 + z_R^2)} |u|^2 \\ p_\phi &= \varepsilon_o \frac{\omega l}{r} |u|^2 \\ p_z &= \varepsilon_o \omega k |u|^2 \end{aligned} \tag{19}$$

where  $\varepsilon_o$  is dielectric permittivity,  $\omega$  is angular frequency,  $k$  is the wavenumber,  $r$  is the radius from the OAM beam axis,  $z_R$  is the Rayleigh range of the Gaussian beam,  $u(r, \phi, z) = u(r, z)\exp(il\phi)$  is the amplitude, and  $l$  is the integer topological charge. For a well-collimated beam we take  $p_r = 0$ . The Poynting vector then takes on the skew angle  $\gamma = l/kr$ , where  $\gamma = \tan^{-1}(p_\phi/p_z)$ .<sup>13</sup>

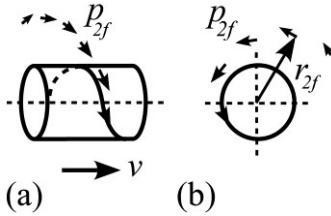


FIG. 8. (a) A HS from Fig. 5(c) following the path of a right-wound Sp-2 helix, moves around the tube at speed  $c$  and from left to right with speed  $v < c$ . As the HS runs along the helical trajectory a spiral momentum field  $p_{2f}$  propagates outward radially. This must have a linear and an azimuthal component. (b) Right-end elevation of Fig. 8(a) in its propagation direction with field radius  $r_{2f}$ . The field arrow length is proportional to the magnitude of the azimuthal momentum.

While an OAM beam consists of a chaos of photons, we might assume by analogy for the present exposition that the skew angle for the trajectory of a *single* HS is obtained from the following relationships:

$$p_\phi = \frac{l\hbar}{r}, \quad p_z = \frac{h}{\lambda} \tag{20}$$

We now posit that a Sp-2 structure with angular momentum  $\hbar$  affects the surrounding space as it rotates, so that its curvature generates a spiral field, see Fig. 8. Its azimuthal momentum shall be given by

<sup>13</sup> Leach *et al.* give the small angle approximation  $\gamma = p_\phi/p_z$  for the case  $l = 1$ ,  $\lambda = 6.32 \times 10^{-7}$ m, and  $r = 10^{-3}$ m, to yield  $\gamma = 6.32 \times 10^{-4}$ rads [43].

$$p_{2f} = \frac{\hbar}{r_{2f}} \quad (21)$$

where  $r_{2f}$  is the field radius from the Sp-2 center. This we shall denote the ‘magnetic-momentum field’ which only results from a Sp-2 rotation. Viewed in the propagation direction, there are two Sp-2 rotation senses: clockwise and counter-clockwise. We shall also assume without further analysis that at a sufficiently large distance  $r_{2f}$  from the Sp-2 axis the spiral magnetic momentum field approaches the target without curvature, that is, in straight parallel lines perpendicular to the line joining the source and target.

This shall be our model of the electron (e.g. cathode rays) and the proton, the difference being only one of scale. The innovation here is that electrons always possess a magnetic-momentum field even when stationary and confined to a closed-circle Sp-2 loop. Electrons moving along a conduction wire in a potential gradient have parallel axes and so their magnetic-momentum fields reinforce, circulating the wire. This contradicts the Maxwell–Heaviside electrodynamics [57] which requires that the electron must be in relative motion to create a magnetic field. In the new model, the lack of motion in a conduction wire with no potential gradient produces randomly orientated electrons whose magnetic-momentum field vectors conspire to cancel out. However, we should keep in mind that the Maxwell–Heaviside theory was conceived over 30 years before evidence for the electron first appeared [58],<sup>14</sup> and over 70 years before light rays were demonstrated to possess spin angular momentum [13].<sup>15</sup>

## 2.6. Response to fields

Here, we provide a brief sketch of the magnetic and electric momentum fields. The electron and proton, since they have Sp-2 rotation, can generate a magnetic-momentum field in the surrounding space but they are unable to produce an electric-momentum field. This will require a further curvature (Sp-3) applied to the Sp-2 axis, see Section 2.7. However, they are to be capable of *responding* to the rotation of both fields. Here, they interact so that the field and Sp-2 momenta will be additive.

The external electric-momentum field receives a closer examination in Section 4.1.1. For the present, we can summarize it by stating that we have a Sp-3 field rotation with either the same or opposite sense to that of the PTV. If the Sp-3 rotations have the opposite sense there a reduction in resident Sp-3 momentum; if they have the same sense there is an increase. We posit that the resident action in Sp-2 or Sp-3, whether reduced (attraction) or increased (repulsion) by the intruding field, when affected by a field will tend to the next lowest integer action. With an attraction, the PTV moves towards the source to increase the field effect and reduce the resident action further. For repulsion, the field moves away from the source to reduce the field effect and attempt to reduce the action to its original value. However, the axis of the external (source) rotation must penetrate the Sp-3 aperture.

The Lorentz force acting on a Sp-2 circuit when passing through an external magnetic-momentum field has been treated elsewhere [59].

## 2.7. Sp-3 rotation (toroidal)

### 2.7.1 PTV construction

A PTV is now to be constructed by bending the z-axis of the trajectory in Fig. 5(c) into a closed loop.<sup>16</sup> The rotation about the poloidal and toroidal axes are to be denoted Sp-2 and Sp-3, respectively. An ‘unloaded’ PTV denotes one that has absorbed no radiation. This is shown in Fig. 9(a), with constant Sp-3 radius  $R_3$ , and an

<sup>14</sup> Thomson [58] measured the charge-to-mass ratio of cathode rays in an evacuated tube.

<sup>15</sup> Beth [13] used a suspended half-wave plate to reverse the rotation sense of circularly polarized light and create a measureable reaction in the plate.

<sup>16</sup> It is not a new idea that an electron or proton is a trapped circular polarized photon, in which its linear momentum is given toroidal circulation [60]. However, the photon has previously been represented in terms of electric fields (instead of it being the basis of them), and no energy levels of a hydrogen atom have yet been calculated.

average Sp-3 azimuthal speed  $v_3 = \beta = \alpha c$ , see Fig. 9(b). Here, we have set  $\beta = \alpha$  the fine structure constant. The HS passes around the guide-tube shown in Fig. 5(c) at speed  $c$  and after curving the  $z$ -axis this tube progresses along the Sp-3 ring in Fig. 9(c) at average toroidal speed  $v_3$ .

There is now an opportunity to introduce the electric momentum as

$$p_3 = m_2 v_3 = m_2 \alpha c \quad (22)$$

where  $m_2$  is given by Eq. (10). In Fig. 9(a), the Sp-2 field momentum is shown as  $p_{2f}$  (magnetic) and the Sp-3 field momentum as  $p_{3f}$  (electric). The two fields result from the dual curvature of the HS trajectory, about the poloidal and toroidal axes, respectively. Using Eq. (12) with  $\beta = \alpha$ , the ‘unloaded’ action for the Sp-2 and Sp-3 rotations is to be

$$J_2 = h = m_2 c (1 - \alpha^2)^{1/2} \cdot 2\pi R_2, \quad J_3 = h = m_2 \alpha c \cdot 2\pi R_3 \quad (23)$$

where  $m_2$  is given by Eq. (10) and  $2\pi R_2 = c T_2 (1 - \beta^2)^{1/2}$ . It follows from Eq. (23) and the values in Table 3 that the electron Sp-3 ring radius  $R_3 = 5.29 \times 10^{-11}$  m and the proton Sp-3 ring radius  $R'_3 = 2.88 \times 10^{-14}$ , having represented the proton radius with a primed quantity. If we also represent Eq. (23) in primed (proton) variables and use Eq. (10) then we also have

$$\frac{R'_2}{R_2} = \frac{R'_3}{R_3} = \frac{m_o}{m'_o} = M, \quad \frac{R_2}{R_3} = \frac{R'_2}{R'_3} = \frac{\alpha}{(1 - \alpha^2)^{1/2}} \quad (24)$$

Since the Sp-2 azimuthal rotation for a single trapped photon has action  $h$  and the tube also has motion along the  $z$  axis then it must have absorbed energy, see Sec. 2.4.5.<sup>17</sup> Since the absorption of radiation energy is not being considered at present, then it must have arisen from electrostatic repulsion.

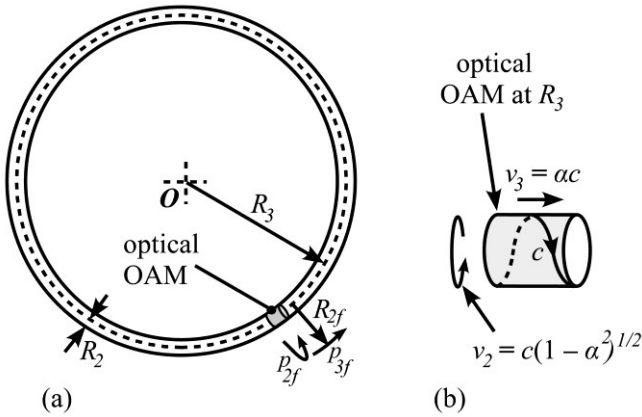


FIG. 9 (a) An unloaded PTV for a single trapped photon with average Sp-3 radius  $R_3$ , which represents the average-radius closed-circle trajectory that the Sp-2 trajectory follows. As the HS follows its guide tube at speed  $c(1 - \alpha^2)^{1/2}$  around the poloidal axis of the toroid, it progresses around the toroidal axis  $O$  at average speed  $\alpha c$ . Here,  $p_{2f}$  and  $p_{3f}$  are the Sp-2 and Sp-3 magnetic and electric field momenta, respectively. (b) Enlarged view of the Sp-2 tube (optical OAM) from Fig. 9(a), around which a HS progresses, where  $v_2$  and  $v_3$  are the Sp-2 and Sp-3 HS velocity components, respectively.

### 2.7.2 Momentum fields

By analogy with the azimuthal momentum in Eq. (20), using Eq. (23) we can write the magnitude of the magnetic momentum field as

<sup>17</sup> If it had not absorbed energy and had merely been stretched out by an attractive field then the action  $h$  would be the total of the azimuthal and linear action.

$$|\vec{p}_{2f}| = \frac{\hbar}{R_{2f}} = m_{2f}v_2 = \left(m_2 \frac{R_2}{R_{2f}}\right) c(1 - \alpha^2)^{1/2} \quad (25)$$

Here, we elect to keep the speed of the field an invariant, and allow the mass  $m_{2f}$  it carries, to diminish with  $R_{2f}$ . Similarly, we can generalize the Sp-3 momentum in Eq. (22) as

$$|\vec{p}_{3f}| = \left(m_2 \frac{R_2}{R_{2f}}\right) \alpha c \quad (26)$$

so that combining (25) and (26)

$$|\vec{p}_{3f}| = \frac{|\vec{p}_{2f}| \alpha}{(1 - \alpha^2)^{1/2}} \quad (27)$$

Equation (27) is independent of  $R_{2f}$ . The Sp-2 field momentum  $\vec{p}_{2f}$  in Eq. (25) is tangential to the Sp-2 rotation about the poloidal  $z$  axis, see Fig. 9(a). The Sp-3 field momentum  $\vec{p}_{3f}$  in Eq. (26) acts tangentially to the curved  $z$  axis perpendicular to  $\vec{p}_{2f}$ . Since the two components are always mutually perpendicular, the square of the resultant field speed becomes

$$v_{2f}^2 + v_{3f}^2 = c^2(1 - \alpha^2) + (\alpha c)^2 = c^2 \quad (28)$$

So while the field momentum is inversely proportional to  $R_{2f}$ , the speed of the field remains  $c$  everywhere. Similarly, from Eqs (25) and (26) we have

$$|\vec{p}_{2f}|^2 + |\vec{p}_{3f}|^2 = \left(m_2 \frac{R_2}{R_{2f}}\right)^2 c^2 \quad (29)$$

Although there is conservation of Sp-2 angular momentum in the field, there is no conservation for Sp-3, because the radius  $R_{3f}$  of this rotation is taken from the toroidal not the poloidal axis, see Fig. 9(a).

### 2.7.3 Self-potential

Electron vortices have been prepared in the laboratory by providing pre-existing electron plane waves with a spiral phase structure [61–63]. No external central potential is needed for electrons to adopt quantized states [10]. So, the PTV model presented here will now introduce an internal potential that depends on the toroidal radius. After division of Eq. (23) by  $2\pi R_3$  and multiplication by  $v_3 = \alpha c$ , we arrive at the Sp-3 toroidal energy of motion

$$\varepsilon_3 = m_2 \alpha^2 c^2 = \frac{\hbar \alpha c}{R_3} \quad (30)$$

Here, we assume the total energy is  $p_2 v_2$  for Sp-2 and  $p_3 v_3$  for Sp-3, which is Eq. (28) multiplied by the PTV mass  $m_2$ . Eq. (30) shall serve as a ‘self-potential’ term which we add to the rest mass energy as follows:

$$m_{pot} c^2 = m_o c^2 + m_2 \alpha^2 c^2 = m_o c^2 + \frac{\hbar \alpha c}{R_3} \quad (31)$$

where  $m_2$  is given by Eq. (10) and  $m_{pot}$  includes the self-potential energy. This amounts to an overload of energy (action per unit time) in the Sp-2 rotation and its redistribution into linear motion, which here adopts a

Sp-3 curvature. This will be an important contribution to Eq. (35) and an accurate fine structure formula in Eq. (54).

#### 2.7.4 Field structure

Figure 10(a), which is not to scale, shows a proton PTV (left) on a common toroidal  $x$  axis with an electron PTV (right). Eq. (24) gives the relative size of the two PTV. The proton Sp-2 field momentum  $\vec{p}'_{2f}$  strikes the electron Sp-2 circuit B at A over the shortest distance  $R'_{2f}$ . This is shown in more detail in Fig. 10(b). The magnitude of this magnetic field momentum falls off inversely as  $R'_{2f}$ , see Eq. (25). We shall assume that in the locality of B, the magnetic momentum field lines from the proton source are straight, parallel, perpendicular to the line joining the proton-electron Sp-2 centers, and in the same plane as the electron toroidal axis  $x$ . The vector  $\vec{p}'_{2f}$ , the line  $R'_{2f}$ , and the  $x$  axis are coplanar, see Fig. 10(b). In contrast, the Sp-3 field momentum vector  $\vec{p}'_{3f}$  runs tangential to the electron poloidal axis at B and is perpendicular to the  $x$  axis, see Fig. 10(a). From Eq. (29), the magnetic-momentum field (from Sp-2) and the electric-momentum field (from Sp-3) are merely the components of a resultant field that has speed  $c$ . These fields are constructed from the motion of a photon as vector components; the photon is not the manifestation of the motion of fields.

Let us now parametrize the position A of the HS on the Sp-2 cross-section B in relation to the origin of the electron toroid as follows, see Fig. 10(b):

$$\vec{R}_{3f} = \begin{pmatrix} R_2 \cos \gamma \\ (R_3 + R_2 \sin \gamma) \sin \theta \\ (R_3 + R_2 \sin \gamma) \cos \theta \end{pmatrix} \quad (32)$$

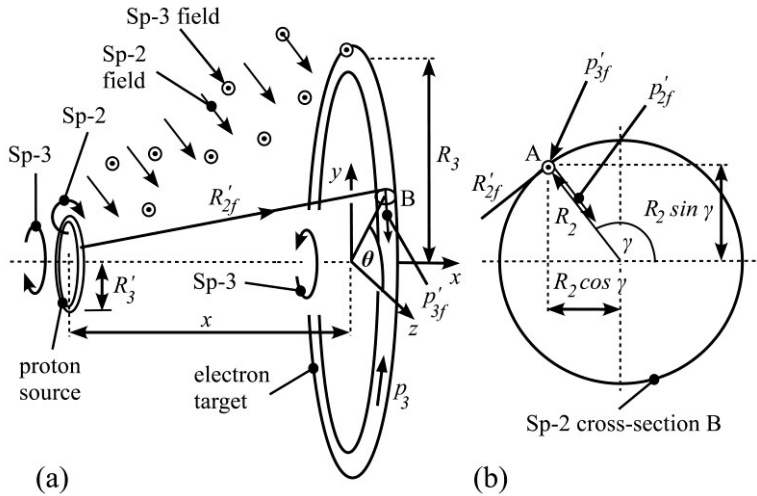


FIG. 10 (a) A proton PTV (left) with Sp-3 radius  $R'_3$  and an electron PTV target (right) with Sp-3 radius  $R_3$ . (b) Expanded view of electron Sp-2 cross-section at B. An arbitrary point on the Sp-2 cross-section is denoted by A.

The constant radius  $R_3$  extends to the curved poloidal axis.<sup>18</sup> Since there are now two mutually perpendicular axes of curvature — poloidal and toroidal — the momentum field takes on a dual-spiral structure. In Fig. 11, a proton PTV is shown in which  $p'_{2f}$  is the magnetic momentum and  $p'_{3f}$  is the electric momentum in the proton's field. These momenta are mutually perpendicular.

<sup>18</sup> More precisely, to the average Sp-3 radius.

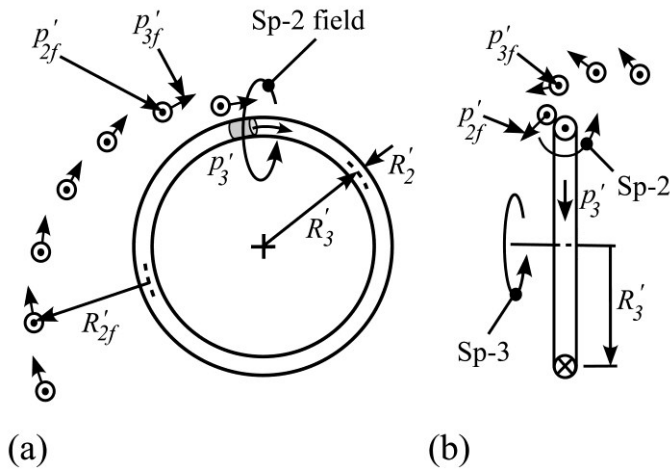


FIG. 11 The proton's spiral momentum field. The dotted circles are magnetic-momentum field components running out of the page while crosses are into the page. (a) The Sp-3 model with Sp-2 and Sp-3 field-momentum components  $p'_{2f}$  and  $p'_{3f}$ , respectively. The variable Sp-2 field radius is  $R'_{2f}$ . (b) Right-end elevation of the PTV. The Sp-2 magnetic momentum (arrowed) and Sp-3 electric momentum (dotted) field components are mutually perpendicular.

The linear momentum of a HS is the same for the two Sp-1 rotation senses, and so there are only two different chiralities for PTVs arising from the two possible Sp-2 rotation senses.<sup>19</sup>

### 3. THE 'LOADED' PTV MODEL

#### 3.1. The notional tube

By 'loaded' ring we mean a PTV that has absorbed radiation. Our focus will now be on the electron PTV, and we posit two effects.

*Stimulated absorption.* The frequency associated with the Sp-3 rotational energy of motion is reduced when the rotation of the incident radiation opposes the Sp-3 motion, in the target PTV. Having reduced frequency, the electron moves to a higher level.

*Stimulated emission.* The frequency is increased when the radiation rotates in the same sense. Having an increased frequency, the electron moves to a lower energy level provided it is not already in ground state.

However, whether circular or elliptical, whatever the total quantum number  $n$ , its toroidal axis will remain parallel to the axis of a tube with constant radius  $r_{3o}$ , see Fig. 12.<sup>20</sup> All energy levels are to operate on the same notional tube. These processes require no external potential.

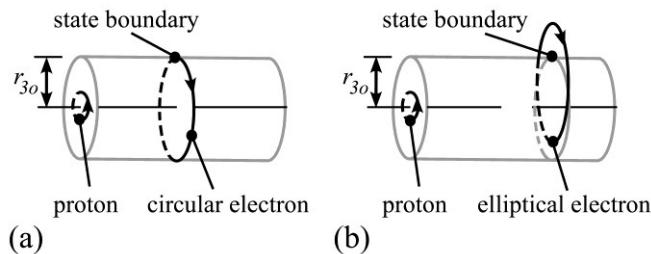


FIG. 12 Both circular and elliptical Sp-3 forms (PTVs) are derived from the same notional tube with radius  $r_{3o}$ , see Eq. (67).

<sup>19</sup> The two Sp-2 rotation senses arise from the azimuthal rotation of the HS.

<sup>20</sup> In Fig. 12, for the elliptical levels, if the normal electron PTV is not parallel to the proton normal then the proton Sp-3 momentum field does not present its maximum effect, a requirement for the derivation of Coulomb's law in Section 4.1.1.

We next derive an energy-level formula for an electron in a field-free region of space. We shall then place the toroidal vortex in the external field of a proton at the entry to a bound state, see Section 4.1.1, and derive the hydrogen fine-structure formula, see Section 3.2.5. The external electric-momentum field of the proton displaces energy out of the electron PTV into energy of motion which radiates away as the PTV reaches one of the bound-state separation distances. As a matter of notation, the loaded-ring radius will now be given in lower case  $r_3$  in contrast to  $R_3$  for the unloaded ring.

### 3.2. Fine structure formula

#### 3.2.1 The mass formula

The effect of the stimulated absorption of radiation with momentum  $p_{rad}$  is to reduce the Sp-3 momentum given by Eq. (31) after division by  $c$  as follows:

$$(mc)^2 = (m_{pot}c)^2 - (p_{rad})^2 \quad (33)$$

where  $m$  is the relativistic radiation-induced mass arising from  $m_{pot}$  and  $p_{rad}$  is the radiation momentum. In a departure from the classical Sommerfeld theory [64], instead of states whose radius  $r_3 \propto n_\phi^2$  we base all states on a notional tube of radius  $r_{3o}$  which can vary if a state is elliptical, see Eq. (67). To this end, we define a string density  $N_3$ . Let the total azimuthal momentum in an electron PTV be given by

$$N_3 p_\phi = \frac{n_\phi \hbar}{r_3} \quad (34)$$

where  $n_\phi \in \mathbb{Z}^+$  is Sommerfeld's azimuthal quantum number,  $p_\phi$  is the azimuthal momentum of a single HS, the function  $N_3(n_\phi, n_r, \theta)$  is the number of HS (string density), and  $n_r$  is Sommerfeld's radial quantum number [64].<sup>21</sup>

Let the radial momentum for a single HS be  $p_r$  then using Eq. (31) we require Eq. (33) to produce the momentum of a single string as follows:

$$(mc)^2 = \left( m_o c + \frac{\hbar \alpha}{N_3 r_3} \right)^2 - (p_{rad})^2, \quad (p_{rad})^2 = \left( \frac{n_\phi \hbar}{N_3 r_3} \right)^2 + (p_r)^2 \quad (35)$$

Rearranging Eq. (35) yields

$$p_r = \left( \frac{\hbar^2 (\alpha^2 - n_\phi^2)}{(N_3 r_3)^2} + \frac{2m_o \hbar \alpha c}{N_3 r_3} + (m_o^2 - m^2) c^2 \right)^{1/2} \quad (36)$$

We now set up the action integral with the radial quantum number  $n_r = 0, 1, 2, \dots$  as follows:

$$\oint p_r d(N_3 r_3) = n_r h \quad (37)$$

assuming that  $N_3$  is not a function of  $r_3$ . Using the integral solution [64] we have

$$\oint \left( \frac{C}{(N_3 r_3)^2} + \frac{2B}{N_3 r_3} + A \right)^{1/2} d(N_3 r_3) = -2\pi i \left( \sqrt{C} - \frac{B}{\sqrt{A}} \right) = n_r h \quad (38)$$

Noting the possibilities that  $i(\alpha^2 - n_\phi^2)^{1/2} = (n_\phi^2 - \alpha^2)^{1/2}$  and  $i/(m_o^2 - m^2)^{1/2} = -1/(m^2 - m_o^2)^{1/2}$ , it follows that

<sup>21</sup> Equation (34) is an innovation and does not appear in the Sommerfeld theory. It introduces a density of strings and leads to all circular states lying on a notional tube having the same radius. Sommerfeld has no function  $N_3(n_\phi, n_r, \theta)$  but instead has the radius  $r_3$  proportional to  $n_\phi^2$  in Eq. (65).

$$m = \frac{m_o}{\left(1 - \frac{\alpha^2}{Y^2 \left(1 + \frac{\alpha^2}{Y^2}\right)}\right)^{1/2}} = m_o \left(1 + \frac{\alpha^2}{Y^2}\right)^{1/2} \quad (39)$$

where  $Y = n_r + (n_\phi^2 - \alpha^2)^{1/2}$ . This differs from Eq. (40), which is Sommerfeld's fine structure equation, in which the sign of the half power is altered [64] as follows:

$$m = m_o \left(1 + \frac{\alpha^2}{Y^2}\right)^{-1/2} \quad (40)$$

In consequence, one might imagine that Eq. (39) is in error, however, we shall see that when we introduce the energy displaced out of the electron PTV due to the intruding proton electric-momentum field — see Sec. 4.1.1 — then Eq. (39) is precisely the required form to set up the new hydrogen atom calculation.

### 3.2.2. Sp-2 and Sp-3 speed

We note that for  $n_r = 0$  (no radial variation) and  $n_\phi = 1$ , Eq. (39) becomes

$$m = \frac{m_o}{(1 - \alpha^2)^{1/2}} \quad (41)$$

Comparison of Eqs. (39) and (41) suggests that the Sp-3 speed transforms from the ground state  $(n_r, n_\phi) = (0, 1)$  to general quantum numbers  $(n_r, n_\phi)$  as follows:

$$v_3 = \alpha c \rightarrow \frac{\alpha c}{Y \left(1 + \frac{\alpha^2}{Y^2}\right)^{1/2}} \quad (42)$$

We then take the Sp-2 speed to be

$$v_2 = \frac{c}{\left(1 + \frac{\alpha^2}{Y^2}\right)^{1/2}} \quad (43)$$

so that from Eqs. (42) and (43) the speed of a HS in a PTV is the speed of light in a vacuum

$$v = \sqrt{v_2^2 + v_3^2} = c \quad (44)$$

### 3.2.3 Sp-2 and Sp-3 momentum

Using Eqs. (39) and (43), the Sp-2 momentum of a string is

$$p_2 = mv_2 = m_o \left(1 + \frac{\alpha^2}{Y^2}\right)^{1/2} \frac{c}{\left(1 + \frac{\alpha^2}{Y^2}\right)^{1/2}} = m_o c \quad (45)$$

indicating that it is independent of the quantum numbers. From Eqs. (39) and (42) the average Sp-3 momentum is

$$p_3 = mv_3 = m_o \left(1 + \frac{\alpha^2}{Y^2}\right)^{1/2} \frac{\alpha c}{Y \left(1 + \frac{\alpha^2}{Y^2}\right)^{1/2}} = \frac{m_o \alpha c}{Y} \quad (46)$$

The magnitude of the HS momentum for a single trapped photon in the PTV is then

$$p = \sqrt{p_2^2 + p_3^2} = m_o c \left(1 + \frac{\alpha^2}{Y^2}\right)^{1/2} \quad (47)$$

### 3.2.4 Energy of Sp-3 motion

Using Eqs. (42) and (46), the energy (action per unit time) contained in the Sp-3 (electric-momentum) component on a stationary field-free mass ring is

$$\mathcal{E}_3 = p_3 v_3 = mv_3^2 = m_o \left(1 + \frac{\alpha^2}{Y^2}\right)^{1/2} \frac{\alpha^2 c^2}{Y^2 \left(1 + \frac{\alpha^2}{Y^2}\right)} = \frac{m_o \alpha^2 c^2}{Y^2 \left(1 + \frac{\alpha^2}{Y^2}\right)^{1/2}} \quad (48)$$

This is the energy of a single HS or trapped photon in a PTV that is free from external fields.

### 3.2.5 Sommerfeld–Dirac energy levels

The fine structure spectral formula is to result from considering only the electric momentum (Sp-3). Let us now rewrite Eq. (48) as

$$\mathcal{E}_3 = \frac{m_o}{\left(1 - \frac{\alpha^2}{Y^2 \left(1 + \frac{\alpha^2}{Y^2}\right)}\right)^{1/2}} \frac{\alpha^2 c^2}{Y^2 \left(1 + \frac{\alpha^2}{Y^2}\right)} \quad (49)$$

which brings out the dependence of  $\mathcal{E}_3$  on  $v_3$ , see Eqs. (39) and (42).

Consider a proton and an electron PTV approaching each other on a common toroidal axis in order to form a bound state, see Fig. 10. At a certain distance apart — their fixed separation in the bound state — let us posit the rake angle of the helical trajectory of the electron to be  $\pi/4$ . This means that both the Sp-3 speed of the electron component remaining in the PTV and its displaced speed in a helical trajectory towards the proton are

$$v_3 = \frac{\alpha c}{\sqrt{2Y \left(1 + \frac{\alpha^2}{Y^2}\right)^{1/2}}} \quad (50)$$

Then  $\mathcal{E}_3$  in Eq. (49) transforms to

$$\mathcal{E}_3 = \frac{m_o}{\left(1 - \frac{\alpha^2}{2Y^2 \left(1 + \frac{\alpha^2}{Y^2}\right)}\right)^{1/2}} \frac{\alpha^2 c^2}{2Y^2 \left(1 + \frac{\alpha^2}{Y^2}\right)} \quad (51)$$

We now expand Eq. (51) up to fourth order in  $\alpha$ . Considering an expansion of  $Y^2$  in powers of  $\alpha$  we note that

$$Y^{-2} = \left( n_r + (n_\phi^2 - \alpha^2)^{1/2} \right)^{-2} = \frac{1}{n^2} \left( 1 + \frac{\alpha^2}{nn_\phi} + \frac{\alpha^4}{n^2 n_\phi^2} \left( \frac{n_r}{4n_\phi} + 1 \right) + \dots \right) \quad (52)$$

where  $n = n_r + n_\phi$ , and consequently we obtain the expansion of Eq. (51) as

$$\mathcal{E}_3 \sim \frac{m_o \alpha^2 c^2}{2Y^2} \left( 1 + \frac{\alpha^2}{4Y^2} \left( 1 - \frac{\alpha^2}{Y^2} \right) + \frac{3\alpha^4}{32Y^4} + \dots \right) \left( 1 - \frac{\alpha^2}{Y^2} + \frac{\alpha^4}{Y^4} + \dots \right) \quad (53)$$

Using Eq. (52), up to sixth order in  $\alpha$  this becomes

$$\mathcal{E}_3 \sim \frac{m_o \alpha^2 c^2}{2n^2} \left( 1 + \frac{\alpha^2}{n^2} \left( \frac{n}{n_\phi} - \frac{3}{4} \right) + \frac{\alpha^4}{n^4} \left( \frac{n_r n^2}{4n_\phi^3} + \frac{n^2}{n_\phi^2} - \frac{3n}{2n_\phi} + \frac{19}{32} \right) + \dots \right) \quad (54)$$

which agrees exactly with the Sommerfeld–Dirac fine structure formula to fourth order in  $\alpha$  [65]. There is also good agreement to sixth order. Of these four terms, in the first, the traditional result gives an extra  $n$  in place of  $n_r$ ; the coefficient of the second term is  $3/4$  instead of  $1$ ; and the last term is  $5/8$  instead of  $19/32$ . The comparison is given in Table 1, using the CODATA from Table 3 in the Appendix, where  $n$ ,  $L$ , and  $spin$  are the traditional total, orbital angular momentum, and spin quantum numbers. The quantum numbers  $(n_r, n_\phi)$  are taken from the Sommerfeld theory [64]. This is the energy of one string as depicted in Fig. 13(a).<sup>22</sup>

TABLE 1. Comparison of a selection of fine-structure energy levels (MHz) of atomic hydrogen as given by the Sommerfeld–Dirac theory (top), against the new PTV theory (bottom) without reduced mass adjustment, see Eq. (54).

State	$n$	$L$	$spin$	$n_\phi$	$n_r$	Sommerfeld (top) against PTV (bottom) MHz
$1S_{1/2}$	1	0	+1/2	1	0	3 289 885 758.5350 3 289 885 758.2606
$2S_{1/2}$	2	0	+1/2	1	1	822 474 177.0559 822 474 177.0455
$2P_{1/2}$	2	1	-1/2	1	1	822 474 177.0559 822 474 177.0455
$2P_{3/2}$	2	1	+1/2	2	0	822 463 227.3948 822 463 227.3973
$3S_{1/2}$	3	0	+1/2	1	2	365 542 862.0518 365 542 862.0545
$3P_{1/2}$	3	1	-1/2	1	2	365 542 862.0518 365 542 862.0545
$3P_{3/2}$	3	1	+1/2	2	1	365 539 617.7225 365 539 617.7107
$3D_{3/2}$	3	2	-1/2	2	1	365 539 617.7225 365 539 617.7107
$3D_{5/2}$	3	2	+1/2	3	0	365 538 536.3069 365 538 536.2900
$4S_{1/2}$	4	0	+1/2	1	3	205 617 346.6448 205 617 346.6404
$4P_{1/2}$	4	1	-1/2	1	3	205 617 346.6448

<sup>22</sup> In Fig. 13(a), a string is composed of 4 sub-strings so Eq. (54) gives their total energy. Figure 13(b) suggests that with 4 strings there is 4 times the energy given by Eq. (54) — which is correct — but a detector would very likely be triggered by only one such string.

						205 617 346.6404
$4P_{3/2}$	4	1	+1/2	2	2	205 615 977.9509
						205 615 977.9344
$4D_{3/2}$	4	2	-1/2	2	2	205 615 977.9509
						205 615 977.9344
$5S_{1/2}$	5	0	+1/2	1	4	131 594 869.7183
						131 594 869.7178
$6S_{1/2}$	6	0	+1/2	1	5	91 385 208.5955
						91 385 208.5862

The reduced mass is not included in the fine-structure calculations in Table 1. The relations between the traditional quantum numbers and Sommerfeld's that govern the new PTV calculations are  $n_\phi = L + spin + 1/2$  and  $n_r = n - n_\phi$ .

### 3.2.6. Sp-3 radial and intensity functions

We now again consider Eq. (35) to solve for  $N_3 r_3$  as follows:

$$(mc)^2 = \left(m_o c + \frac{\hbar\alpha}{N_3 r_3}\right)^2 - \left(\frac{n_\phi \hbar}{N_3 r_3}\right)^2 - \left(m \frac{dr_3}{dt}\right)^2 \quad (55)$$

where  $r_3$  is the Sp-3 radius — which can be elliptic — and  $p_r = m dr_3/dt$  is the radial momentum of a single HS.<sup>23</sup> The starting point is to use azimuthal ( $\theta$ ) angular momentum conservation. Using Eq. (34)

$$m \frac{dr_3}{dt} = m \frac{d\theta}{dt} \frac{dr_3}{d\theta} = \frac{n_\phi \hbar}{N_3 r_3^2} \frac{dr_3}{d\theta} = \frac{n_\phi \hbar}{(N_3 r_3)^2} \frac{d(N_3 r_3)}{d\theta} \quad (56)$$

assuming that  $N_3$  is independent of  $\theta$ . We then set up  $d(N_3 r_3)/d\theta$  to arrive at the following integral:

$$\int d\theta = \int \frac{d(N_3 r_3)}{(N_3 r_3) R^{1/2}} \quad (57)$$

where

$$R = a + b(N_3 r_3) + c(N_3 r_3)^2 \quad (58)$$

and

$$\begin{aligned} a &= \frac{\alpha^2}{n_\phi^2} - 1 < 0 \\ b &= \frac{2m_o \alpha c}{n_\phi^2 \hbar} \\ c &= -\frac{m_o^2 \alpha^2 c^2}{Y^2 n_\phi^2 \hbar^2} \end{aligned} \quad (59)$$

<sup>23</sup> Here, all circular states have the same PTV radius, see Eq. (63), independently of the quantum numbers.

having used Eq. (39).

The solution for this integral form [66] is

$$\int \frac{dx}{xR^{1/2}} = \frac{1}{\sqrt{-a}} \sin^{-1} \left( \frac{2a + bx}{x(b^2 - 4ac)^{1/2}} \right); \quad a < 0; b^2 - 4ac > 0 \quad (60)$$

where  $x = N_3 r_3$ . Then

$$N_3 r_3 = \frac{-2a}{b - (b^2 - 4ac)^{1/2} \sin(\sqrt{-a}\theta)} \quad (61)$$

and

$$N_3 r_3 = \frac{\left(1 - \frac{\alpha^2}{n_\phi^2}\right) n_\phi^2 \hbar}{m_o \alpha c \left[ 1 - \left(1 - \frac{(n_\phi^2 - \alpha^2)}{Y^2}\right)^{1/2} \sin \left( \left(1 - \frac{\alpha^2}{n_\phi^2}\right)^{1/2} \theta \right) \right]} \quad (62)$$

Now the product of  $r_{3o}$  and Eq. (46) at  $n_\phi = 1$ ,  $n_r = 0$ , must be  $\hbar$ . So

$$r_{3o} = \frac{\hbar(1 - \alpha^2)^{1/2}}{m_o \alpha c} \quad (63)$$

For the electron  $r_{3o} = 5.291\ 631\ 210\ 153 \times 10^{-11}$  m, using the values from Table 3. So at  $n_\phi = 1$ ,  $n_r = 0$ , Eq. (62) gives

$$N_{3o} = (1 - \alpha^2)^{1/2} \quad (64)$$

We determine the function  $N_3$  for the circular states ( $n_r = 0$ ) from Eq. (62) as follows

$$N_3 r_3 = \frac{\left(1 - \frac{\alpha^2}{n_\phi^2}\right) n_\phi^2 r_{3o}}{(1 - \alpha^2)^{1/2}} \quad (65)$$

Since we propose that  $r_3 = r_{3o}$  for all circular states then using Eq. (64) the density of HS relative to ground state is

$$\frac{N_3}{N_{3o}} = \frac{\left(1 - \frac{\alpha^2}{n_\phi^2}\right) n_\phi^2}{(1 - \alpha^2)}, \quad N_3 = \frac{\left(1 - \frac{\alpha^2}{n_\phi^2}\right) n_\phi^2}{(1 - \alpha^2)^{1/2}} \quad (66)$$

Let us assume that Eq. (66) applies to elliptic states. From Eqs. (62) and (63) we have

$$r_3 = \frac{r_{3o}}{\left[1 - \left(1 - \frac{(n_\phi^2 - \alpha^2)^{1/2}}{Y^2}\right) \sin\left(\left(1 - \frac{\alpha^2}{n_\phi^2}\right) \theta\right)\right]} \quad (67)$$

It follows from Eq. (67) that the major axis has length  $2r_{3o}Y^2/(n_\phi^2 - \alpha^2)$ . If we consider the elliptic function for  $r_3$  as follows:

$$r_3 = \frac{A(1 - \epsilon_3^2)}{1 - \epsilon_3 \sin(\theta')} \quad (68)$$

with  $\epsilon_3$  as eccentricity, and compare with Eqs. (63) and (67) we have

$$\epsilon_3 = \left(1 - \frac{(n_\phi^2 - \alpha^2)^{1/2}}{Y^2}\right)^{1/2}, \quad A = \frac{\hbar(1 - \alpha^2)^{1/2}Y^2}{(n_\phi^2 - \alpha^2)m_o\alpha c} = \frac{Y^2}{(n_\phi^2 - \alpha^2)}r_{3o}, \quad \theta' = \left(1 - \frac{\alpha^2}{n_\phi^2}\right)^{1/2} \theta \quad (69)$$

All states are based on a notional tube of radius  $r_{3o}$ .

### 3.2.7 Sp-2 action

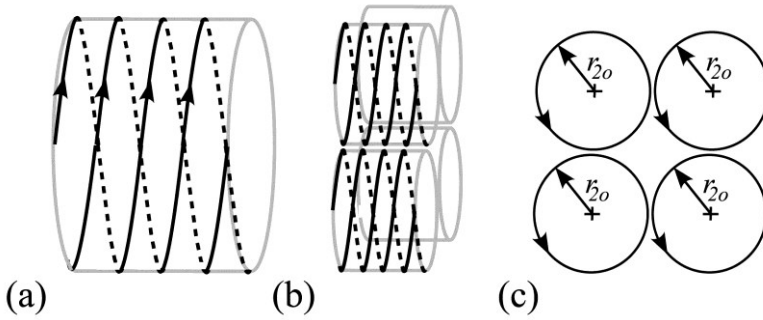


FIG. 13. String density and sub-strings for  $2P_{3/2}$  for which  $n = 2, n_\phi = 2$ . (a) Shown is one of the  $n_\phi^2 = 4$  components of the Sp-2 rotation with  $n = 2$  longitudinal iterations of a HS wavelength, each with  $n = 2$  interlaced parts to give  $n^2 = 4$  sub-strings, so that each has momentum  $m_o c/n^2$ , see Eq. (72); (b) the density of HS components showing  $n_\phi^2 = 4$  tubes as depicted in Fig. 13(a) with Sp-2 radius  $r_{2o}$ ; (c) right-end elevation of the string density in Fig. 13(b).

In experiments involving optical OAM, which is equivalent to Sp-2 here,<sup>24</sup> interlaced fronts affect the angular momentum quantum number  $n_\phi$ , see Soskin *et al.* [19] and Marucci *et al.* who state “the wave front of this field is composed of  $|m|$  intertwined helical surfaces [...]” [67]. Using Sommerfeld’s quantum numbers we have  $n_\phi = |m|$ . This occurs without radiation absorption. Using Eqs. (1) and (63) we have

$$r_{2o} = \frac{\alpha}{(1 - \alpha^2)^{1/2}} r_{3o} \quad (70)$$

For any Sp-2 circuit that has either been affected by a repulsion field — see Eq. (16) — or has absorbed radiation, we take the physical radius  $r_2$  to be an invariant, so

$$r_2 = r_{2o} \quad (71)$$

The total Sp-2 action Eq. (6) is as follows, keeping Eqs. (45) and (71) in mind:

$$h = n^2 \int_0^{2\pi} \frac{m_o c r_{2o}}{n^2} d\gamma \quad (72)$$

This reconfiguration follows the above discussion on interlaced circuits. Each of the  $n_\phi^2$  string tubes is to consist of  $n$  longitudinal wavelengths, each with  $n$  interlaced circuits — see Fig. 13(a) — to produce  $n^2$  circuits or sub-strings in each tube. Each sub-string is to carry a Sp-2 momentum  $m_o c / n^2$ , see Eq. (72). The idea of longitudinal iteration and the reduced time period will be useful for the derivation of Coulomb’s law in Sec. 4.1.1.<sup>25</sup>

For the Sp-3 angular momentum  $N_3 / N_{3o} \sim n_\phi^2$ , where  $n_\phi$  is the azimuthal quantum number, see Eq. (66). The Sp-3 circular radius is an invariant  $r_{3o}$  so that the increase in Sp-3 angular momentum  $n_\phi \hbar$  with an increase in  $n_\phi$  arises from an increase in string density not Sp-3 radius as Sommerfeld had it [2]. Although each of the  $n_\phi^2$  strings has the same energy — given here by Eq. (51) — and is capable of registering at a detector, the low probability of coincident registrations renders the duplicated energy virtually inaccessible [51].

## 4. THE HYDROGEN ATOM

### 4.1. Coulomb’s law for bound states

---

<sup>24</sup> The difference is that the optical OAM produced in the laboratory consists of redirected rectilinear rays (see Fig. 1) whereas the posited OAM or Sp-2 here relies on a photon following a curvilinear trajectory.

<sup>25</sup> It is also in anticipation of a theory of hyperfine structure in preparation.

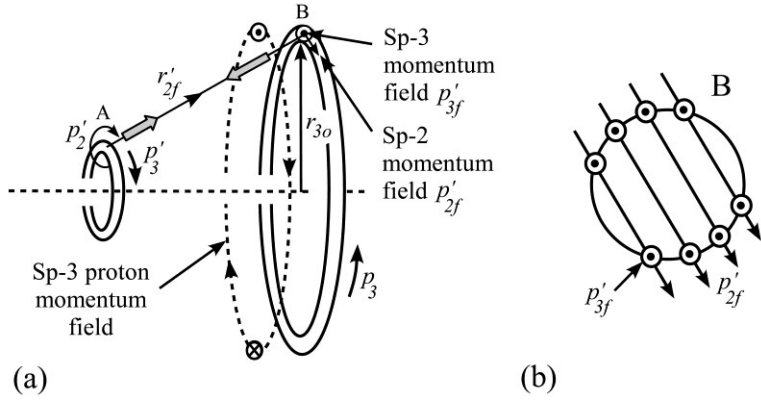


FIG. 14 (a) The proton PTV (left) and the electron PTV (right). Momentum out of the page is indicated by a dot and into the page by a cross. The proton Sp-3 field momentum  $p'_{3f}$  at B sourced from A has the opposite rotation sense to the electron momentum  $p_3$  in the electron PTV thus creating an attractive force. (b) Closer view of the electron Sp-2 circuit at B with the proton's intersecting magnetic momentum  $p'_{2f}$  and electric momentum  $p'_{3f}$  fields.

The reason that the PTV acquires energy of motion is that the external electric momentum field that penetrates and opposes its rotation sense, reduces the resident Sp-3 energy and redistributes it along  $r'_{2f}$  towards the proton A, see Fig. 14(a) and Section 3.1. In the nineteenth century, MacCullagh [68] suggested that a rotationally elastic ether carries a potential energy per unit volume that depends on its rotational kinetic energy. A similar idea will be invoked here as we discuss the effect of the proton's  $p'_{3f}$  electric-momentum field as it intersects the Sp-2 circuit of the electron along its circuit normal and tangential to the poloidal axis, see Eq. (26).

#### Assumptions of the model

- (1) At every point in space at which a magnetic-momentum field vector  $\vec{p}'_{2f}$  occurs there is an accompanying electric-momentum field vector  $\vec{p}'_{3f}$  vector perpendicular to it, see circuit B in Fig. 14(b) and Eq. (29).
- (2) The rotation senses of these two field vectors follow the Sp-2 and Sp-3 senses determined at their point of origin A.
- (3) The magnetic-momentum  $\vec{p}'_{2f}$  cannot pass through the toroidal axis, dotted horizontally in Fig. 14(a), since it is confined to the half-plane containing the point of origin of the fields A and the toroidal axis of the proton.
- (4) The  $\vec{p}'_{2f}$  vectors in the locality of the electron Sp-2 circuit B, being the result of a spiral field, occur in straight quasi-parallel lines perpendicular to the line joining the proton-electron Sp-2 centers.<sup>26</sup>
- (5) The electron Sp-2 circuit normal or angular momentum vector runs perpendicular to the electron PTV toroidal axis even if the Sp-3 motion follows a helical trajectory around that axis due to motion of the PTV.

*Electrical attraction.* In Fig. 14(a), which is not to scale, a proton PTV and an electron PTV with opposite Sp-3 rotation senses and common toroidal axes are shown in close proximity. In consequence, the proton electric momentum inhabiting the electron PTV has the opposite sense to the electron Sp-3 rotation so reduces the resident action. The azimuthal Sp-3 action now tends to reduce so there is motion towards the source. The proton's Sp-3 momentum field  $p'_{3f}$  displaces an equal energy out of the electron PTV at B into linear motion of the electron along  $r'_{2f}$  towards the proton.<sup>27</sup> So, the axis of the Sp-2 trajectory at B takes on a helical path with both a reduced azimuthal (Sp-3) component and a displaced component along  $r'_{2f}$ , while adhering to Assumption (5) above. Emissions occur from this displaced energy when the proton–electron system reaches

<sup>26</sup> In the model presented here, the momentum vectors proceed radially in a spiral pattern — see Fig. 11 — which we assume to be approximately linear in the locality of the target.

<sup>27</sup> We might assume that axis of the Sp-2 circuit representing the electron iteratively runs an incremental distance along  $r'_{2f}$  then an increasing radial increment along  $r_{3o}$  to restore the original Sp-3 radius.

their bound state separation distance, see Section 4.1.2. There must be a reciprocal action, with B affecting A, where the proton motion resulting from the displacement out of the ring at A moves along  $r'_{2f}$  towards the electron. Being of negligible effect, we shall not consider this case any further here. Electrical attraction, in which energy is not added to the electron, but displaced as a conservative field is analogous to the passive acceleration introduced in Section 2.3.6.

*Electrical repulsion.* In the hydrogen atom, there is no repulsion of energy out of the electron ring. However, when repulsion occurs in a system, the electric momentum field and Sp-3 momentum rotate in the same sense, are additive, and so there is an action overload in the Sp-3 circuit. The PTV retains its resident energy and acquires energy of motion away from the field source in an attempt to reduce the field strength and the momentum overload. Again, the azimuthal Sp-3 action tends to reduce so there is motion away from the source to restore its original value. This is analogous to the active acceleration case in Section 2.4.6 in which case there is an addition of energy.

We now derive Coulomb's law for a proton–electron system for its effect on one of the  $n_\phi^2$  strings that make up an energy level.<sup>28</sup> We recall from Eq. (72) that there are  $n$  longitudinal parts of a string, see Fig. 13(a), a string which receives the following action from the momentum field:

$$J'_{3f} = \int_{\gamma=0}^{\gamma=2\pi} \vec{p}'_{3f} \cdot d\vec{r}'_2 \quad (73)$$

Here, the Sp-3 field momentum  $\vec{p}'_{3f}$  acts parallel to the electron's Sp-2 angular momentum vector, see Fig. 14(b). Unlike  $\vec{p}'_{2f}$ , which lies in the plane of the Sp-2 circuit and needs a scalar product line integral, the contribution of  $\vec{p}'_{3f}$  is perpendicular to the Sp-2 circuit which received its full magnitude at all points.<sup>29</sup> So we take its direction to mirror that of  $d\vec{r}'_2$ , thus from Eqs. (21) and (27) we have

$$\vec{p}'_{3f} = \frac{\hbar\alpha}{r'_{2f}(1-\alpha^2)^{1/2}} \begin{pmatrix} -\sin\gamma \\ \cos\gamma \\ 0 \end{pmatrix} \quad (74)$$

where from Fig. 10(b), using lower case for the 'loaded' case, we have

$$d\vec{r}'_2 = r_{2o}d\gamma \begin{pmatrix} -\sin\gamma \\ \cos\gamma \\ 0 \end{pmatrix} \quad (75)$$

Following Fig. 10 we have

$$r'_{2f} = ((x + r_{2o} \cos\gamma)^2 + (r_{3o} - r'_{3o} + r_{2o} \sin\gamma)^2)^{1/2} \quad (76)$$

which becomes

$$r'_{2f} = (x^2 + (r_{3o} - r'_{3o})^2 + r_{2o}^2 + 2r_{2o}(x \cos\gamma + (r_{3o} - r'_{3o}) \sin\gamma))^2)^{1/2} \sim (x^2 + (r_{3o} - r'_{3o})^2)^{1/2} \quad (77)$$

This is the distance between the proton-electron Sp-2 centers. If we simply worked with the approximation Eq. (77) there would be no variation in  $\vec{p}'_{3f}$  with  $\gamma$  and no need for a line integral.

Returning to Eq. (73), we have the action acting on the total string in Fig. 13(a) as

$$J'_{3f} = \frac{\hbar\alpha r_{2o}}{(1-\alpha^2)^{1/2}} \int_0^{2\pi} \frac{d\gamma}{r'_{2f}} \quad (78)$$

<sup>28</sup> We recall that each has an energy given by Eq. (51) but we expect only one of the  $n_\phi^2$  strings to register at a detector.

<sup>29</sup> A scalar product line integral involving  $\vec{p}'_{2f}$  is crucial for a hyperfine treatment but is beyond the scope of this work.

Using Eq. (43), the Sp-2 time period  $T_2$  for one longitudinal iteration is

$$T_2 = \frac{2\pi r_{2o}}{v_2} = \frac{2\pi n r_{2o} \left(1 + \frac{\alpha^2}{Y^2}\right)^{1/2}}{c} \quad (79)$$

Since there are  $n$  interlaced components in one longitudinal iteration or Sp-2 circuit and there are  $n^2$  components in total — see Fig. 13(a) — the proportion of the action absorbed in the electron time period  $T_2$  for one circuit of these interlaced components must be  $1/n$ .<sup>30</sup> So dividing (78) by  $T_2$  and taking  $\hbar$  from Eq. (23) with  $m_2 = m_o$ ,  $R_3 = r_{3o}$ , we obtain from Eq. (77) the proton-field energy absorbed by a single electron HS, as follows:<sup>31</sup>

$$\varepsilon'_{3f} = \frac{\hbar \alpha c}{2\pi n \left(1 + \frac{\alpha^2}{Y^2}\right)^{1/2} (1 - \alpha^2)^{1/2}} \int_0^{2\pi} \frac{d\gamma}{r'_{2f}} \sim \frac{m_o \alpha^2 c^2 r_{3o}}{n(x^2 + (r_{3o} - r'_{3o})^2)^{1/2}} \quad (80)$$

We now concern ourselves with accuracy and write Eq. (80) as

$$\varepsilon'_{3f} = m_o \alpha^2 c^2 F'(x) \quad (81)$$

with

$$F'(x) = \frac{r_{3o}}{2\pi n (1 - \alpha^2) \left(1 + \frac{\alpha^2}{Y^2}\right)^{1/2}} \int_0^{2\pi} \frac{d\gamma}{r'_{2f}} \quad (82)$$

#### 4.2 State boundaries

We have already seen in Fig. 14(a) that as the electron PTV approaches the proton ring from outside their bound state, the electron and proton Sp-2 trajectories are directed towards each other along  $r'_{2f}$ . The electron PTV can be either circular or elliptic. The normal vector at the electron's Sp-3 circle center or elliptic focus is to run along the axis of a notional tube with radius  $r_{3o}$  (the radius of all states) given by Eq. (63), see Fig. 12. This ensures that the interacting proton field momentum  $p'_{3f}$  always acts in the plane of the electron PTV.

In Fig. 14(a), when the electron PTV in its lowest state approaches the proton PTV from the right, the proton electric-momentum field that inhabits it, displaces an equivalent energy into energy of motion. This is radiated away at the separation boundary as ionization energy thereby bringing the electron PTV to rest. Thereafter, when the electron adopts higher energy states — which possess lower frequencies — the boundary B moves further away from the proton, retaining radius  $r_{3o}$  on the tube.<sup>32</sup> Our aim now is to obtain the proton-electron fixed separation distance for each bound state.

Considering Fig. 10 and Eqs. (76) and (77), we have

$$\frac{r_{3o}}{r'_{2f}} = \frac{1}{(1 - \bar{r}'_{3o}) \left(1 + \frac{\bar{x}^2 + \bar{r}'_{2o}{}^2}{(1 - \bar{r}'_{3o})^2}\right)^{1/2}} \left(1 + \frac{2\bar{r}'_{2o}}{(1 - \bar{r}'_{3o})^2} \frac{(\bar{x} \cos \gamma + (1 - \bar{r}'_{3o}) \sin \gamma)}{\left(1 + \frac{\bar{x}^2 + \bar{r}'_{2o}{}^2}{(1 - \bar{r}'_{3o})^2}\right)}\right)^{-1/2} \quad (83)$$

Here  $r_{3o}$  from Eq. (63) is independent of the quantum numbers, and we have made use of it to produce the following normalizations — see Table 3 in the Appendix:

<sup>30</sup> It should be noted that  $n$  could replace  $n^2$  in Eq. (72) and would be simpler but the given reconfiguration has been chosen in anticipation of a theory of hyperfine structure still in development.

<sup>31</sup> Note that at any point in our derivation we can substitute  $\hbar \alpha c = e^2/4\pi\epsilon_o$ , using Eq. (30) with  $m_2 = m$  and  $R_3 = r_{3o}$ .

<sup>32</sup> At least, the circular states stay on the surface of the tube. The elliptic states described by Eq. (67) have a major axis related to  $r_{3o}$ .

$$\bar{x} = \frac{x}{r_{3o}}, \quad \bar{r}'_{3o} = \frac{r'_{3o}}{r_{3o}} = \frac{r'_{2o}}{r_{2o}} = \frac{m_o}{m'_o} = M, \quad \bar{r}_{2o} = \frac{r_{2o}}{r_{3o}} = \frac{\alpha}{(1 - \alpha^2)^{1/2}} \quad (84)$$

having used Eq. (70) and replaced the upper-case (unloaded PTV) with lower-case (loaded PTV) variables in Eq. (24). Here,  $\bar{x}$  is the co-axial proton–electron separation distance, which is normalized by being expressed as a fraction of the electron Sp-3 invariant radius  $r_{3o}$ .

The first task is to execute the integral in Eq. (82) to fourth order in  $\alpha$  using the binomial series, and demand that at a bound state separation distance, the proton field energy in the electron ring energy is half of the total remaining electron ring energy. This equality is given by the equivalence of Eq. (51) with Eqs. (81) and (82) in the center of mass frame, so that

$$\begin{aligned} & \frac{1}{n(1 - \alpha^2) \left(1 + \frac{\alpha^2}{Y^2}\right)^{1/2} (1 - \bar{r}'_{3o}) \left(1 + \frac{\bar{x}^2 + \bar{r}'_{2o}{}^2}{(1 - \bar{r}'_{3o})^2}\right)^{1/2}} \left( 1 + \frac{3\bar{r}'_{2o}{}^2(\bar{x}^2 + (1 - \bar{r}'_{3o})^2)}{4(1 - \bar{r}'_{3o})^4 \left(1 + \frac{\bar{x}^2 + \bar{r}'_{2o}{}^2}{(1 - \bar{r}'_{3o})^2}\right)^2} \right. \\ & \quad \left. + \frac{105\bar{r}'_{2o}{}^4(\bar{x}^2 + (1 - \bar{r}'_{3o})^2)^2}{64(1 - \bar{r}'_{3o})^8 \left(1 + \frac{\bar{x}^2 + \bar{r}'_{2o}{}^2}{(1 - \bar{r}'_{3o})^2}\right)^4} + \dots \right) \\ & = \frac{1}{2(Y^2 + \alpha^2) \left(1 - \frac{\alpha^2}{2Y^2 \left(1 + \frac{\alpha^2}{Y^2}\right)}\right)^{1/2}} \end{aligned} \quad (85)$$

A brute-force search is now conducted for the  $\bar{x}$  that satisfies Eq. (85) for a particular set of quantum numbers. This is the stationary separation of the proton- electron Sp-2 centers in a bound state, and is expressed as a fraction of the invariant electron Sp-3 tube radius  $r_{3o}$ . The values of  $\bar{d}_2$  are recorded in Table 2 as the normalized distances between the proton and electron Sp-2 centers (distance AB in Fig. 14) where

$$\bar{d}_2 = (\bar{x}^2 + (1 - M)^2)^{1/2} \quad (86)$$

having noted Eq. (84). As can be seen from Table 2,  $\bar{d}_2 \sim 2n$ . This linear dependence on  $n$  is to be crucial for the hyperfine separation calculation presently in development and is the main reason why the Sommerfeld radial dependence on  $r_3 \propto n_\phi^2$  has been abandoned in favour of a density function, see Eqs. (63)–(68).

TABLE 2. The normalized proton–electron separation  $\bar{d}_2$  of the Sp-2 centers at the hydrogen state boundary using Eqs. (85) and (86). The actual distance is  $\bar{d}_2 r_{3o}$ , see Eq. (63).

State	$\bar{d}_2$ at state boundary	State	$\bar{d}_2$ at state boundary
$(n_r = 0)$		$4P_{3/2}/4D_{3/2}$	8.000 381 100 130
$1S_{1/2}$	2.000 033 283 609	$5D_{5/2}/5F_{5/2}$	10.000 503 695 795
$2P_{3/2}$	4.000 176 404 340	$(n_r = 3)$	
$3D_{5/2}$	6.000 295 116 857	$4S_{1/2}/4P_{1/2}$	8.000 327 844 976
$4F_{7/2}$	8.000 407 727 308	$5P_{3/2}/5D_{3/2}$	10.000 485 944 315
$5G_{9/2}$	10.000 517 896 931	$6D_{5/2}/6F_{5/2}$	12.000 609 094 719
$(n_r = 1)$		$(n_r = 4)$	
$2S_{1/2}/2P_{1/2}$	4.000 123 149 485	$5S_{1/2}/5P_{1/2}$	10.000 432 689 104
$3P_{3/2}/3D_{3/2}$	6.000 277 365 407	$6P_{3/2}/6D_{3/2}$	12.000 591 343 232
$4D_{5/2}/4F_{5/2}$	8.000 398 851 598	$(n_r = 5)$	
$(n_r = 2)$		$6S_{1/2}/6P_{1/2}$	12.000 538 087 983
$3S_{1/2}/3P_{1/2}$	6.000 224 110 351	$7P_{3/2}/7D_{3/2}$	14.000 697 059 139

### 4.3 Reduced mass

So far, the calculation for the bound-state separation distance has been referred to the electron's center of mass frame. However, if instead we compute the electron mass relative to the proton, our answer must relate to the stretching out of the Sp-2 helix representing the electron mass along its poloidal axis relative to a stationary proton field in the locality of the electron. This rotating field occupies the electron PTV ring and runs in the opposite direction to the electron Sp-3 motion along the poloidal axis, see Fig. 14(a). The difficulty lies in the comparison of proton field flow speed and electron mass-energy speed because they are computed by different means. In fact, the concept of 'field-flow form' is novel here. The difference between field-flow form and mass-energy form is that the former must be integrated around a Sp-2 circuit to obtain the latter. So we must consider how to convert the electron energy in Eq. (51) from mass-energy form to field-flow form. Since the electron Sp-2 axis remains perpendicular to the toroidal axis as the Sp-3 motion takes on a helical trajectory about the toroidal axis, then noting Eqs. (1), (24), (70), (74), and the division by  $n$  in Eq. (80), we have the uniformly distributed proton field momentum that is absorbed by the electron as follows:<sup>33</sup>

$$|\vec{p}'_{3f}| = \frac{m'_o M \alpha^2 c r_{3o}}{n r'_{2f} (1 - \alpha^2)} \sim \frac{m'_o M \alpha^2 c}{2n^2 (1 - \alpha^2)} \quad (87)$$

having noted that Table 2 suggests that the  $r'_{2f}/r_{3o}$  is given by  $\bar{d}_2 \sim 2n$ . Equation (87) is an example of momentum in field-flow form.

We now focus on Eq. (51). This is the electron motion in mass-energy form and is the energy carried by a Sp-2 circuit. To convert it into momentum field-flow form for comparison with Eq. (87), we divide by  $v_2$ . Thus Eq. (51) becomes

$$p_{3f} = \frac{\mathcal{E}_3}{v_2} = \frac{m_o}{\left(1 - \frac{\alpha^2}{2Y^2 \left(1 + \frac{\alpha^2}{Y^2}\right)}\right)^{1/2}} \frac{\alpha^2 c}{2Y^2 \left(1 + \frac{\alpha^2}{Y^2}\right)^{1/2}} \quad (88)$$

having used Eq. (43). We now compute the flow speeds from Eqs. (87) and (88) by dividing by the proton and electron relativistic masses  $m'_o$  and  $m$  respectively to find

$$v'_{3f} \sim \frac{M \alpha^2 c}{2n^2 (1 - \alpha^2)} \quad (89)$$

and

$$v_{3f} = \frac{\alpha^2 c}{2Y^2 \left(1 + \frac{\alpha^2}{Y^2}\right)^{1/2}} \quad (90)$$

---

<sup>33</sup> Again, only a fraction  $1/n$  of the field momentum is absorbed in the electron time period.

Equation (89) is the proton momentum field flow speed and Eq. (90) is the electron momentum flow speed. Since  $Y \sim n$ , this leaves us with the approximate, though significant relationship

$$v'_{3f} \sim Mv_{3f} \quad (91)$$

The reduced mass of the electron  $\mu$  now follows from this analysis of field flow speeds in the electron PTV since in order to conserve momentum we must have

$$\mu(v'_{3f} + v_{3f}) = mv_{3f}, \quad \mu = \frac{m}{1 + M} \quad (92)$$

having made use of Eq. (91). The advantage of this calculation over a simple conservation of angular momentum principle, is that there is a visualizable mechanism at work in the locality of the electron.

## 5. CONCLUSIONS

A new model for the electron, proton, and their bound state has been suggested based on the classical Sommerfeld fine-structure theory and recent work on optical OAM. The calculation makes use of the Sommerfeld quantum numbers to derive accurate fine structure energies.

(1) The proton and electron have an identical form (their difference being only scale), namely, a density of helical strings each with two rotation types (Sp-2 and Sp-3) as a photonic toroidal vortex (PTV). The string length in the PTV is inversely proportional to its mass, see Eq. (1). Contrary to the Sommerfeld–Dirac derivations [2, 4], a PTV can possess energy levels in the absence of an external field due to a self-potential resulting from its Sp-3 energy.

(2) In the PTV, the poloidal rotation (Sp-2) represents magnetic momentum and the toroidal rotation (Sp-3) represents electric momentum. Each rotation generates a spiral momentum field. All rotations that construct mass and field run at the speed of light  $c$ . However, the mass in the field varies inversely as the distance from its Sp-2 center.

(3) As the electron approaches the proton along their common toroidal axis, the oppositely rotating Sp-3 proton momentum field  $p'_{3f}$  inhabiting the electron PTV displaces resident momentum  $p_3$  along  $r'_{2f}$ . When the bound state separation distance  $\bar{d}_2$  is reached at a rake angle of  $\pi/4$  this energy of motion is radiated away. Coulomb's law is derived in this analysis, see Section 4.1.1. The Sp-2 angular momentum vector remains perpendicular to the toroidal axis, even when the PTV is in motion and the Sp-2 center adopts a helical trajectory.

(4) Contrary to Sommerfeld's scheme in which the Sp-3 radius  $r_3 \sim n_\phi^2$  [2], all circular electron states are centered on the same notional tube of radius  $r_{3o}$ . For elliptic states, the Sp-3 angular momentum vector must be aligned with the tube axis otherwise the proton electric momentum field has a reduced effect.

(5) The number of HS tubes in a level is  $n_\phi^2$ -fold, as shown in Fig. 13(b). In a bound state, each of the  $n_\phi^2$  HS — as shown in Fig. 13(a) — possesses the total energy given by Eq. (51). A 'single photon' is to consist of a parallel array of many strings, each with the same energy and each capable of exciting a detector. However, the probability of two strings in this array coincidentally exciting spatially separate detectors can be as low as  $7.5 \times 10^{-4} - 5.3 \times 10^{-2}$  [51]. So even though there are  $n_\phi^2$  tubes with the same energy, the most likely scenario is that only a single tube will be absorbed by a detector.

(6) Each of the  $n_\phi$  strings consists of  $n$  longitudinally-joined sub-strings each with  $n$  interlaced strings making  $n^2$  sub-strings. A sub-string carries Sp-2 momentum  $m_o c/n^2$ , see Eq. (72). This assumption assists in the derivation of Coulomb's law and is given in anticipation of a future theory of hyperfine structure.

For the  $1S_{1/2}$  state in hydrogen, the experimental value of 1 420.405 751 768(1) MHz can be compared with the QED result of 1 420.452 MHz [69, Table 4]. The error is less than 4 parts in  $10^5$ . A paper on applying the PTV model to the Lamb shifts and hyperfine separations is in preparation. A preliminary PTV calculation for the separation between the two  $1S_{1/2}$  hyperfine states gives 1 420.813 MHz, an error of less than 3 parts in  $10^4$ . Although this is slightly less accurate than QED, the PTV calculation relies on a single calculation rather than several *ad hoc* correction terms.<sup>34</sup>

TABLE 3. 2018 CODATA values for constants used [70].

symbol	constant	CODATA value
$\alpha$	Fine structure constant	0.007 297 352 569 3
$c$	Speed of light in vacuum	299 792 458 ( $ms^{-1}$ )
$g_p$	Landé g-factor for proton	5.585 694 689
$m_o$	Rest mass electron	$9.109 383 701 5 \times 10^{-31}$ ( $kg$ )
$m'_o$	Rest mass proton	$1.672 621 923 695 \times 10^{-27}$ ( $kg$ )
$M$	Rest mass electron/proton	0.000 544 617 021 488
$h$	Planck's constant	$6.626 070 15 \times 10^{-34}$ ( $J Hz^{-1}$ )
$Ry$	Rydberg frequency <sup>35</sup>	3 289 841 960.250 86 ( $MHz$ )
$\pi$	pi	3.141 592 653 589 793

## REFERENCES

1. N. Bohr, On the constitution of atoms and molecules, London, Edinburgh, and Dublin Philosophical Magazine, **26** (July 1913): 1–25.
2. A. Sommerfeld, Zur quantentheorie de spektrallinien, Annalen der Physik **51** (1916): 125–167.
3. P. A. M. Dirac, The quantum theory of the electron, Proceedings of the Royal Society of London A **117** (1928): 610–624.
4. C. G. Darwin, The wave equations for the electron, Proceedings of the Royal Society of London A **118** (1928): 654–680.
5. W. E. Lamb and R. C. Retherford, Fine structure of the hydrogen atom, Physical Review **72**, 3 (1947): 241–243.
6. H. A. Bethe, L. M. Brown, and J. R. Stehn, Numerical value of the Lamb shift, Physical Review **77**, (1950): 370.
7. M. I. Eides, H. Grotch, and V. A. Shelyuto, Theory of light hydrogen atoms, Physics Reports **342** (2001): 63–261.
8. M. Uchida, and A. Tonomura, Generation of electron beams carrying orbital angular momentum, Nature **464** (2010): 737–739. (doi:10.1038/nature08904)
9. J. Veerbeck, H. Tian, and P. Schattschneider, Production and application of electron vortex beams, Nature **467** (2010): 301–304. (doi: 10.1038/nature09366)
10. B. J. McMorran, A. Agrawal, I. M. Anderson, A. A. Herzing, H. J. Lezec, J. J. McClelland and J. Unguris, Electron vortex beams with high quanta of orbital angular momentum, Science **331** (2011): 192–95. (doi:10.1126/science.1198804)
11. S. M. Lloyd, M. Babiker, G. Thirnavukkarusa, and J. Yuan, Electron vortices – beams with orbital angular momentum, Review of Modern Physics **89**, 035004. (doi: 10.1103/RevModPhys.89.035004)
12. K. Y. Bliokh, I. P. Ivanov, G. Guzzinati, L. Clark, R. Van Boxem, A. Béché, R. Juchtmans, M. A. Alonso, P. Schattschneider, F. Norri, and J. Veerbeck, Theory and applications of free-electron vortex states, Physics Reports **690** (2017): 1–70. (doi: 10.48550/arXiv.1703.06879)
13. R. A. Beth, Mechanical detection and measurement of the angular momentum and light, Physical Review **50** (1936): 115–25.
14. D. N. Moothoo, J. Arlt, R. Conroy, F. Akerboom, A. Voit, and K. Dholkia, Beth's experiment using optical tweezers, American Journal of Physics **69** (2001): 271–276.
15. P. J. Allen, A radiation torque experiment, American Journal of Physics **34** (1966): 1185–1192.
16. B. A. Garetz and S. Arnold, Variable frequency shifting of circularly polarized laser radiation via a rotating half-wave retardation plate, Optical Communications **31** (1979): 1–3.
17. F. Bretenaker and A. Le Floch, Energy exchanges between a rotating retardation plate and a laser beam, Physical Review Letters **65** (1990): 2316–7.

<sup>34</sup> PTV requires a single calculation. See Kramida (2010) for a summary of the QED corrections [73, Sec. 3].

<sup>35</sup> Calculated from  $Ry = 0.5 \times m_o \alpha^2 c^2 \times 10^{-6}/h$ .

18. M. W. Beijersbergen, R. P. C. Coerwinkel, M. Kristensen, and J. P. Woerdman, Helical wavefront laser beams produced with a spiral phaseplate, *Optics Communications* **112** (1994): 321–27.
19. M. S. Soskin, V. N. Gorshkov, M. V. Vasnetsov, J. T. Malos, and N. R. Heckenberg, Topological charge and angular momentum of light beams carrying optical vortices, *Physical Review A* **56** (1997): 4064–4075, Fig. 5.
20. D. Y. Tang, N. R. Heckenberg, and C. O. Weiss, Phase dependent helical pattern formation in a laser, *Optics Communications* **114** (1995): 95–100.
21. H. He, M. E. J. Friese, N. R. Heckenberg, and H. Rubinsztein-Dunlop, Direct observation of transfer of angular momentum to absorptive particles from a laser beam with a phase singularity, *Physical Review Letters* **75** (1995): 826–29.
22. J. Courtial, and M. J. Padgett, Performance of a cylindrical mode converter for producing Laguerre–Gaussian modes, *Optics Communications* **159** (1999): 13–18.
23. M. Padgett, J. Arlt, N. Simpson, and L. Allen, An experiment to observe the intensity and phase structure of Laguerre–Gaussian laser modes, *American Journal of Physics* **64** (1996): 77–82.
24. L. Allen, M. W. Beijersbergen, R. J. C. Spreeuw, and J. P. Woerdman, Orbital angular momentum of light and the transformation of Laguerre–Gaussian laser modes, *Physical Review A* **45** (1992): 8185–8189.
25. N. B. Simpson, K. Dholakia, L. Allen, and M. J. Padgett, Mechanical equivalence of spin and orbital angular momentum of light: an optical spanner, *Optics Letters* **22** (January 1997): 52–54.
26. H. A. Haus, *Waves and Fields in Optoelectronics* (New Jersey, Englewood Cliffs, Prentice-Hall 1984).
27. E. Abramochkin and V. Volostnikov, Beam transformations and nontransformed beams, *Optics Communications* **83** (1991): 123–135.
28. M. W. Beijersbergen, L. Allen, H. E. L. O. van der Veen and J. P. Woerdman, Astigmatic laser mode converters and transfer of orbital angular momentum, *Optics Communications* **96** (1993), 123–132.
29. E. Abramochkin and V. Volostnikov, Spiral light beams, *Physics–Uspekhi* **47**, 12 (2004): 1177–1203.
30. D. McGloin and K. Dholakia, Bessel beam: diffraction in a new light, *Contemporary Physics*, **46** (2005): 15–28.
31. M. A. Bandres and J. C. Gutiérrez–Vega, Ince–Gaussian beams, *Optics Letters* **29**, 2 (2004): 144–146.
32. J. C. Gutiérrez–Vega, M. D. Iturbe–Castillo and S. Chávez–Cerdeña, Alternative formulation for invariant optical fields: Mathieu beams, *Optics Letters* **25**, 20 (2000): 1493–1495.
33. X. Hui, S. Zheng, Y. Hu, C. Xu, X. Jin, H. Chi and X. Zhang, Ultraflow reflectivity spiral phase plate for generation of millimetre-wave OAM beam, *IEEE Antennas and Wireless-Propagation Letters* **14** (2015): 966–969.
34. M. E. J. Friese, J. Enger, H. Rubinsztein-Dunlop, N. R. Heckenberg, Optical angular-momentum transfer to trapped absorbing particles, *Physical Review A* **54** (1996): 1593–96.
35. J. Sun, J. Zeng and N. M. Litchinitser, Twisting light with hyperbolic metamaterials, *Optics Express* **21**, 12 (2013): 14975–14981.
36. A. Stefani, R. Lwin, B. T. Kuhlmeiy, and S. C. Fleming, OAM generation, tunable metamaterials and sensors with highly deformable fibers, *Advanced Photonics 2018*, Optica Publishing Group, paper NoTh1D.2, 2018.
37. H. Q. Wei, X. Xue, J. Leach, M. J. Padgett, S. M. Barnett, S. Franke-Arnold, E. Yao, and J. Courtial, Simplified measurement of the orbital angular momentum of single photons, *Optics Communications* **223** (2003): 117–122.
38. J. Leach, J. Courtial, K. Skeldon, Stephen M. Barnett, S. Frank-Arnold, and Miles J. Padgett, Interferometric methods to measure orbital and spin, or the total angular momentum of a single photon, *Physical Review Letters* **92** (2004): 013601.
39. J. Leach, M. J. Padgett, S. M. Barnett, S. Franke-Arnold, and J. Courtial, Measuring the orbital angular momentum of a single photon, *Physical Review Letters* **88** (2002): 257901.
40. A. Mair, A. Vaziri, G. Weihs, and A. Zeiliger, Entanglement of orbital angular momentum states, *Nature* **212** (July 2001): 313–16.
41. J. Leach, S. Keen, M. J. Padgett, C. Saunter, and G. D. Love, Direct measurement of the skew angle of the Poynting vector in a helically phased beam, *Optics Express* **14** (2006): 11919–11924.
42. L. Allen and M. J. Padgett, The Poynting vector in Laguerre–Gaussian beams and the interpretation of their angular momentum density, *Optics Communications* **184** (2000): 67–71.
43. D. Giovannini, J. Romero, V. Potoček, G. Ferenczi, F. Speirits, S. M. Barnett, D. Faccio, and M. J. Padgett, Spatially structured photons that travel in free space slower than the speed of light, *Science* **347**, 6224 (2015): 857–60.
44. A. Aspect, P. Grangier, and G. Roger, Experimental tests of realistic local theories via Bell’s theorem, *Physical Review Letters* **47** (1981): 460–63.
45. P. Grangier, G. Roger, and A. Aspect, Experimental evidence for a photon anticorrelation effect on a beam splitter: a new light on single-photon interferences, *Europhysics Letters* **1** (1986): 173–79.
46. J. Thorn, M. S. Neel, V. W. Donato, G. S. Green, R. E. Davies, and M. Beck, Observing the quantum behaviour of light in an undergraduate laboratory, *American Journal of Physics* **72** (2004): 1210–1219.
47. P. G. Kwiat, E. Waks, A. G. White, I. Appelbaum, and P. H. Eberhard, Ultra-bright source of polarization-entangled photons, *Physical Review A* **60** (1999): 773–76.

48. T.-G. Noh, H. Kim, C. J. Youn, S.-B. Cho, J. Hong, and T. Zyung, Nonlinear correlated photon pair source in the 1550nm telecommunication band, *Optics Express* **14**, 7 (2006): 2805–10.
49. J. Galinis, M. Karpiński, G. Tamošauskas, K. Dobek, and A. Piskarskas, Photon coincidences in spontaneous parametric down-converted radiation excited by a blue LED in bulk LiIO<sub>3</sub> crystal, *Optics Express* **19**, 11 (2011): 10351–10358.
50. M. Ahmed, A. Amponsah, A. Emmanuel, and H. Issake, Source of photon pairs using spontaneous parametric down-conversion process, *International Journal of Innovation and Applied Studies* **9** (2014): 734–43.
51. B. R. Clarke, Reinterpretation of the Grangier experiment using a multiple-triggering single-photon model, *Modern Physics Letters B* **37**, 15, 2350042 (2023).
52. C. Wan, Q. Cao, J. Chen, A. Chong and Q. Zhan, Toroidal vortices of light, *Nature Photonics* **16** (2022): 519–522; Supplementary information <https://doi.org/10.1038/s41566-022-01013-y>, Fig. S5a.
53. J. C. Maxwell, On physical lines of force – Part II, *The Scientific Papers of James Clerk Maxwell*, edited by W. D. Niven (Cambridge University Press, 1890), Vol. 1, p.486.
54. J. H. Poynting, The wave motion of a revolving shaft, and a suggestion as to the angular momentum in a beam of circularly polarized light, *Proceedings of the Royal Society of London A* **82**, 557 (1909): 560–567.
55. J. C. Slater, Spinning electrons and the structure of spectra, *Nature* (24 April 1926), p.587.
56. M. E. J. Friese, J. Enger, H. Rubinsztein-Dunlop, N. R. Heckenberg, Optical angular-momentum transfer to trapped absorbing particles, *Physical Review A* **54** (1996): 1493–1495.
57. J. Clerk Maxwell, A dynamical theory of the electromagnetic field, *Philosophical Transactions of the Royal Society* **155** (1865): 459–512.
58. J. J. Thomson, Cathode rays, *The London, Edinburgh, and Dublin Philosophical Magazine* **44** (1897): 293–316.
59. B. R. Clarke, *The Quantum Puzzle: Critique of Quantum theory and Electrodynamics* (World Scientific Publishing, 2017), pp.267–278, 284–296.
60. W. F. Hagen, Matter in the form of toroidal vortices, *Proceedings of SPIE*, Vol. 9570, 95700T-22 (2015).
61. P. Schattschneider, M. Stöger-Pollach and J. Veerbeck, Novel vortex generator and mode converter for electron beams, *Physical Review Letters* **109** (2012): 084801.
62. E. Mafakheri, A. H. Tavabi, P. -H. Lu, R. Balboni, F. Venturi, C. Menozzi, G. C. Gazzadi, S. Frabboni, A. Sit, R. E. Dunin-Borkowski, E. Karimi, and V. Grillo, Realization of electron vortices with large orbital angular momentum using miniature holograms fabricated by electron beam lithography, *Applied Physics Letters* **110**, 9 (2017): 093113.
63. M. Uchida and A. Tonomura, Generation of electron beams carrying orbital angular momentum, *Nature* **464** (2010): 737–739.
64. A. Sommerfeld, *Atomic Structure and Spectral Lines*, translated into English by Henry Brose (Methuen & Co., 1923), pp.473, 551–52, Appendix A.
65. H. E. White, *Introduction to Atomic Spectra* (McGraw-Hill, 1934), p.134.
66. A. Jeffrey and H.-H. Dai, *Handbook of Mathematical Formulas and Integrals*, 4<sup>th</sup> edition (Amsterdam: Elsevier, 2008), p.173.
67. L. Marrucci, C. Manzo and D. Paparo, Optical spin-to-orbital angular momentum conservation in inhomogeneous anisotropic media, *Physical Review Letters* **96**, 163905 (2006), Fig. 1.
68. J. MacCullagh, An essay towards a dynamical theory of crystalline reflexion and refraction, in *The Collected Works of James MacCullagh*, edited by J. H. Jellett and S. Haughton (Dublin: Hodges, Figgis & Co., 1880), p.145.
69. Kramida, A. E. *Atomic data and nuclear tables*, **96**, (2010): 586–644.
70. E. Tiesinga, P. J. Mohr, D. B. Newell, and B. N. Taylor, CODATA recommended values of the fundamental physical constants: 2018, *Reviews of Modern Physics* **93** (April–June 2021), Tables XXX and XXXI.

**On behalf of all authors, the corresponding author states that there is no conflict of interest. A peer-reviewed and formatted version appears *Quantum Studies: Mathematics and Foundations* **12**, **19** (2025).**

<https://doi.org/10.1007/s40509-025-00364-9>